WATER CHEMISTRY AND LAKE DYNAMICS OF LAGUNA BACALAR, QUINTANA ROO, MEXICO

by

Ryan M. Matzuk

A Thesis Submitted in

Partial Fulfillment of the

Requirements for the Degree of

Master of Science

in Geosciences

at

The University of Wisconsin-Milwaukee

August 2020

ABSTRACT

WATER CHEMISTRY AND LAKE DYNAMICS OF LAGUNA BACALAR, QUINTANA ROO, MEXICO

by

Ryan M. Matzuk

The University of Wisconsin – Milwaukee, 2020
Under the Supervision of Professor Timothy J. Grundl

Laguna Bacalar in the Quintana Roo region is the second largest lake in Mexico and contains freshwater derived solely from groundwater. Local geology on the Yucatan Peninsula is karstic and the southern shoreline of Laguna Bacalar is spotted with a handful of cenotes that contribute substantial amounts of inflowing groundwater to the lake. This is shown by sonde profile data taken in one of the largest cenotes in the area. Outflow is dominated by a surface water outlet in the southern portion of the lake and an unknown amount of outflowing groundwater. During January of 2017 through 2019, UWM researchers collected data on the physical flow to and from the lake, $\delta^{13}C$, $\delta^{18}O$ and $\delta^{2}H$ isotopes, and major ion chemistry in order to provide insight into the overall chemical and physical hydrology of the lake. The primary hydrochemical processes controlling lake chemistry include influx of high alkalinity groundwater in the southern portion, CO_2 evolution and a resultant pH rise and calcite precipitation. Saturation indices modeled using PHREEQC indicate the water in Laguna Bacalar is oversaturated with calcite and at saturation with gypsum. The northern portion of the lake has no groundwater influx and is dominated by evaporative effects. Recently, the lake and the city of Bacalar have gained international attention and are attracting an increasing number of visitors. While fueling a growing tourism industry and economy, this raises the potential for

accelerating human impacts that can threaten the health of this relatively pristine freshwater ecosystem. Understanding the basic hydrology of Laguna Bacalar will be a key element in managing water quality and preserving the truly unique hydrogeological and biological characteristics of the system.

TABLE OF CONTENTS

LIST OF FIGURES

LIST OF TABLES

LIST OF EQUATIONS

LIST OF ABBREVIATIONS

AA	Flame Atomic Absorption Spectrometer, and instrument used to analyze cations
IC	Ion Chromatograph, an instrument used to analyze anions
$\delta^{18}O$	Delta O 18, a measure of the ratio of stable isotopes ^{18}O:^{16}O
$\delta^{2}H$ or δD	Delta H 2, a measure of the ratio of stable isotopes ^{2}H:^{1}H
$\delta^{13}C$	Delta C 13, a measure of the ratio of stable isotopes ^{13}C:^{12}C
MWL	Meteoric Water Line
GMWL	Global Meteoric Water Line
MMWL	Mexican Meteoric Water Line
LEL	Local Evaporation Line
TDS	Total Dissolved Solids
VSMOW	Vienna Standard Mean Ocean Water, an isotopic standard for water
VPBD	Vienna Pee Dee Belemnite, an isotopic standard for carbon
XRD	X-Ray Powder Diffraction, an analytical technique used to determine molecular crystal structures

LIST OF UNITS

atm	Atmosphere
°C	Degrees Celsius
mm	Millimeter
m	Meter
km	Kilometer
m^2	Square meter
m^3	Cubic meter
yr	Year
kg/yr	Kilograms per year
L/yr	Liters per year
m/yr	Meters per year
m^3/yr	Cubic meters per year
m^3/sec	Cubic meters per second
mL	Milliliter
mg	Milligram
mg/L	Milligram per liter
%	Percent
‰	Per mil
meq/L	Milliequivalents per liter
eq/L	Equivalents per liter
mmol/L	Millimoles per liter
N	Normality of standard acid titrant
µS/cm	Microsiemens per centimeter

ACKNOWLEDGEMENTS

I would like to extend special thanks to my advisor Dr. Timothy Grundl for his extensive support with this project and guidance along the way. I would also like to thank my thesis committee members Dr. J. Val Klump and Dr. Shangping Xu for their support and assistance in this project, as well as Jerry Kaster of UWM School of Freshwater Sciences for his extensive knowledge of the Bacalar region and help in the field. Additionally, thank you to Jessie Grow, Dr. Paul Roebber, Maddy Salo, Ruth Fenelon, Ji-In Jung, all other UW-Milwaukee students and faculty that assisted with data collection and analysis for this project, and Martin Maas, our Bacalar point of contact and collaborator. Lastly, I would like to thank the UW-Milwaukee Geosciences department for cultivating my love for the field of geology and allowing me to participate in a multitude of opportunities I would have never had the chance to experience elsewhere.

1. Introduction

Bacalar is a city in the Mexican state of Quintana Roo on the Yucatan Peninsula. The city is located on the west side of Laguna Bacalar, the second largest freshwater lake in the country. Laguna Bacalar is just north of the Belize border on the southeastern side of the Yucatan Peninsula. This lake is comprised entirely of freshwater derived from groundwater inflow. Local geology is karstic, allowing substantial amounts of groundwater to enter the lake through the numerous shoreline cenotes. To this day, very few studies pertaining to the hydrology of the lake have been performed. From 2014 through 2019, UWM researchers collected data on the physical flow, isotopes of dissolved inorganic carbon, oxygen and hydrogen, and overall water chemistry in order to better understand the physical and chemical hydrogeology of this region. This study provides insight into the overall hydrogeologic setting of Laguna Bacalar.

An increasing flux of travelers to the city of Bacalar is threatening the health of this freshwater resource, which is used as a drinking water source and for recreation by locals and tourists alike. This paper aims to assist future water resource decision making practices in the Bacalar region by expanding upon the current breadth of knowledge on hydrochemistry, lake flow dynamics, and water residence times within Laguna Bacalar.

2. Background

The Yucatan Peninsula as a whole is an area of diverse geology mainly due to the ejecta blanket produced by the Chicxulub impactor asteroid. Laguna Bacalar is on the outer skirts of this ejecta blanket and lies primarily on the Neogene-aged Bacalar Formation which is

comprised mainly of limestone. The lake is located approximately 70 km inland from the Gulf of Mexico and the lake body is approximately 42 km long and 1 km wide.

Kenkmann and Schönian (2006) analyzed the Chicxulub crater and subsequent ejecta blanket in the Yucatan Peninsula. One notable finding relating to the general Laguna Bacalar area is the existence of localized pockets of spheroidal dolomite grains within a clay-rich basal portion of the ejecta blanket ranging from 0.1 to 1.7m in thickness underneath the bulk ejecta material. The existence of this basal layer indicates a two-stage stratigraphy of the Chicxulub ejecta blanket with these spheroidal deposits forming during a primary vapor cloud. Due to the somewhat sporadic existence of these pockets, they are either erosional remnants or may be of an alternative origin. While the geology as influenced by the ejecta blanket is variable across the Quintana Roo region, it is noted that in the Bacalar area the lithology is that of fossiliferous marls with occasional re-sedimented ejecta material. The majority of the bedrock in the Laguna Bacalar region is that of the Upper Tertiary Bacalar Formation consisting of limestone with interspersed gypsum. Laguna Bacalar itself contains quaternary aged fluvial deposits consisting of carbonate sediment. Southeast of the city of Bacalar the bedrock is quaternary-aged karst plains.

Sánchez et al. (2016) previously analyzed physiochemical parameters around Quintana Roo in an effort to understand local groundwater quality. The groundwater quality was overall acceptable to be used as drinking water source. The general groundwater flow regime near Laguna Bacalar is moving in the northeast direction parallel to the lake.

Bauer-Gottwein et al. (2011) summarized what is currently understood about the Yucatán Peninsula karst aquifer including challenges associated with hydrological research and

groundwater-resources management in the area. The Yucatan Peninsula encompasses the largest underwater cave systems in the world and groundwater is the sole source of drinking water for most Quintana Roo inhabitants. Furthermore, the hydrogeological properties in the region were modified by the Chicxulub meteorite impact of which ejecta has been located up to ~360km away in Belize in southern Quintana Roo. This ejecta is clay-rich with low hydraulic permeability and is described as having a sealing effect in some regions of the peninsula. Due to the extensive coastline in the area, much of the Yucatan Peninsula is subject to seawater intrusion on the scale of tens of kilometers inland. This restricts the anthropogenic use of groundwater to a freshwater lens with a range of 10 to 100 meters in thickness located within the Yucatan karst aquifer, which is composed of limestones, dolomites, and evaporites. Surface exposed sedimentary rocks in the region range in age from the Upper Cretaceous to Holocene. Preferential flow paths in the region range from 100s of kilometers wide regional-scale fracture zones to small-scale fractures and dissolution cavities in the range of 10s of meters. Laguna Bacalar lies within the boundaries of the Rio Hondo fault zone, which is an extensive horst and graben block fault system off the coast of the southern Yucatan Peninsula that extends on shore and runs nearly parallel to the coastline. This fault system was created from tectonic events during the Late Cretaceous to the Pliocene. Laguna Bacalar occupies one of the larger fault basins in this system.

Perry et al. (2002) described impacts of saltwater intrusion to the geochemical makeup of Yucatan Peninsula groundwater, analyzed flow characteristics of high permeability zones near cenotes and faults in the northern portion of the peninsula, and investigated the influence of precipitants and groundwater chemistry. The area encompassing Laguna Bacalar was

classified as an evaporite region that is characterized as having groundwater high in SO_4 and low in Cl. Laguna Bacalar is fed by groundwater draining from an area rich in gypsum-bearing rocks, most likely Chicxulub impact breccia interspersed in karst bedrock, and is supersaturated with respect to calcite. Although Laguna Bacalar is in close proximity to the coastline, chemical erosion that would otherwise lead to saltwater intrusion does not take place because of this calcite supersaturation and no subsurface groundwater channels or conduits between the Caribbean Sea and Laguna Bacalar are known to exist. If this lake water contacted saltwater it would remain supersaturated with calcite. Since Laguna Bacalar has no direct connection to any saltwater bodies, any freshwater drainage out of the lake likely occurs in the north along the extension of the Rio Hondo fault system (Perry et al. 2002). The underlying chemical process prohibiting erosion is the common ion effect. Groundwater recharge to Laguna Bacalar is coming from areas with high dissolved gypsum and is contributing large amounts of calcium ions to the water, which allows calcite to continue precipitating (Jin et al. 2010).

Lagomasino et al. (2015) focused on the Sian Ka'an Biosphere Reserve, an area of coastal wetlands located approximately 100km north of Laguna Bacalar within the state of Quintana Roo. Life in this area is dependent on the freshwater lens of the Yucatan Peninsula karst aquifer. These researchers used chemical modeling and a coupled principal component analysis and end-member mixing model to identify the sources of groundwater that replenish the wetlands in the reserve. These researchers collected and analyzed major ions, total phosphorus, total nitrogen, and $\delta^{18}O$ and $\delta^{2}H$ isotopes. Using the program PHREEQC, researchers found that all water samples were undersaturated with respect to gypsum and anhydrite and were oversaturated with respect to calcite, dolomite, and aragonite. Using major

ion analyses of collected waters the researchers were able to identify sources of groundwater recharge for various regions of the reserve. This study also notes the phenomenon of differences in pH between subsurface groundwater and surface water recharged from groundwater sources. It is believed that in this area, CO_2 contained in low pH groundwater degasses upon reaching the surface. This serves as a dependable analog for similar processes and differences in pH levels of groundwater and surface water seen in the Bacalar region.

Gondwe et al. (2011) also published a paper focused on the Sian Ka'an Biosphere Reserve. These researchers utilized a Multiple Model Simulation approach to understand the heterogeneity of the Yucatan Peninsula karst aquifer and examine the effects of conceptual model uncertainties on water management decisions. These researchers also reiterate that Laguna Bacalar exists in an area of sub-parallel normal faults with the downthrown side to the east and extensive horst and graben systems present off the eastern coast of the Yucatan Peninsula. Through the models used in this study, researchers demonstrated that conceptual model uncertainty poses a significant issue in determining groundwater sourcing in karst environments, though combining results of multiple models would undoubtedly minimize the degree of uncertainty and would be a critical step in formulating best management practices for groundwater.

3. Site Location

Figure 1 is a map of Yucatan Peninsula bedrock ages and regional-scale fracture zones indicated by red lines. Cenote locations are indicated with red dots (Bauer-Gottwein et al. 2011). The Ring of Cenotes on the northern edge of the Yucatan Peninsula is the outer boundary of the 180 km wide Chicxulub Meteorite Impact Crater. This is a remnant of the meteorite that has been proposed as having led to the downfall of the dinosaurs approximately 65 million years ago (Schönian et al. 2005). Along the east coast of the peninsula exists a handful of major faults which are part of a larger horst and graben system that extends out into the Caribbean Sea (Rozencrantz 1990). Surface water tends to flow parallel to the major faults in the area. The Laguna Bacalar region is on Eocene-aged bedrock.

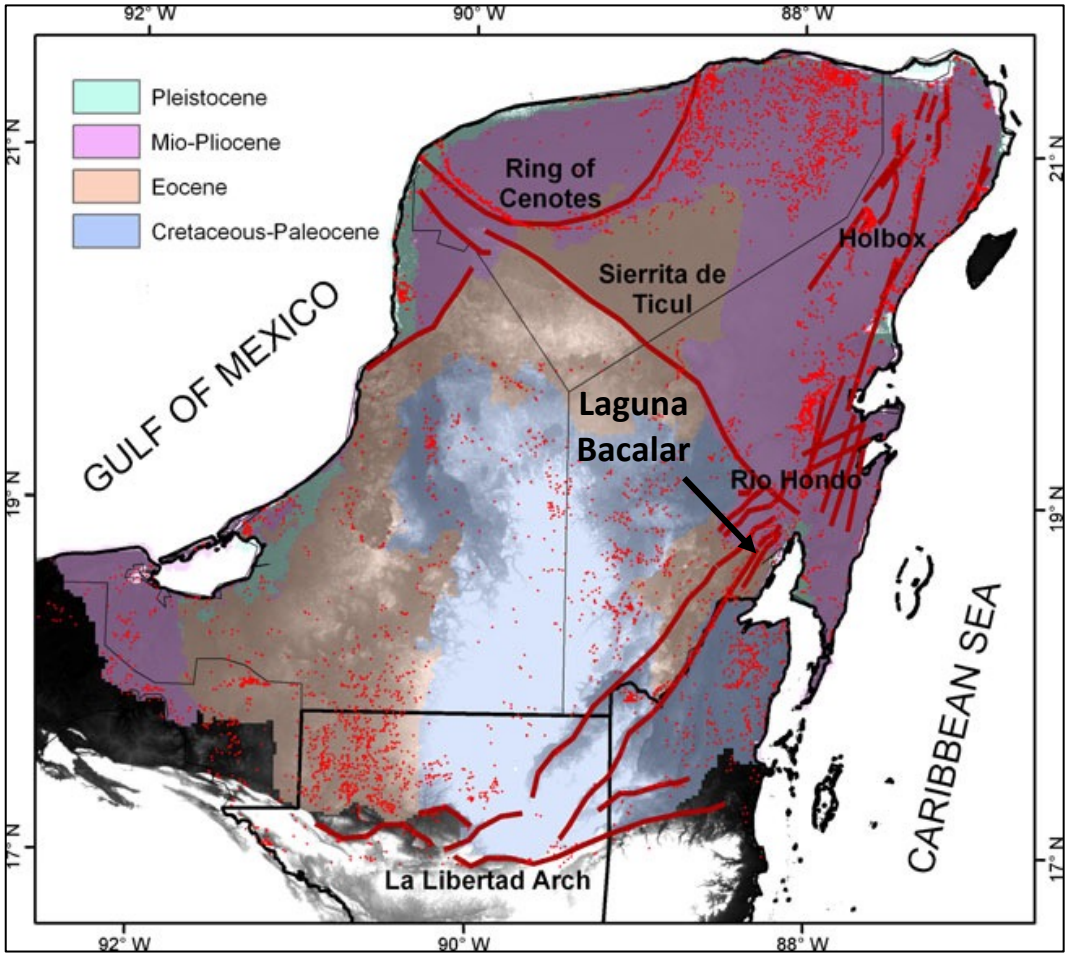

Figure 1. Yucatan Peninsula bedrock ages overlaid with regional-scale fracture zones and cenotes. Bauer-Gottwein et al. 2011.

Figure 2 shows the Yucatan Peninsula with groundwater streamlines in blue as well as elevation where white and black depict high and low elevation, respectively. As expected, groundwater in this region flows down-gradient toward the coastline. Groundwater in the Bacalar region flows along the fault systems in a north/northeastern direction rather than flowing directly to the coast (Bauer-Gottwein et al. 2011).

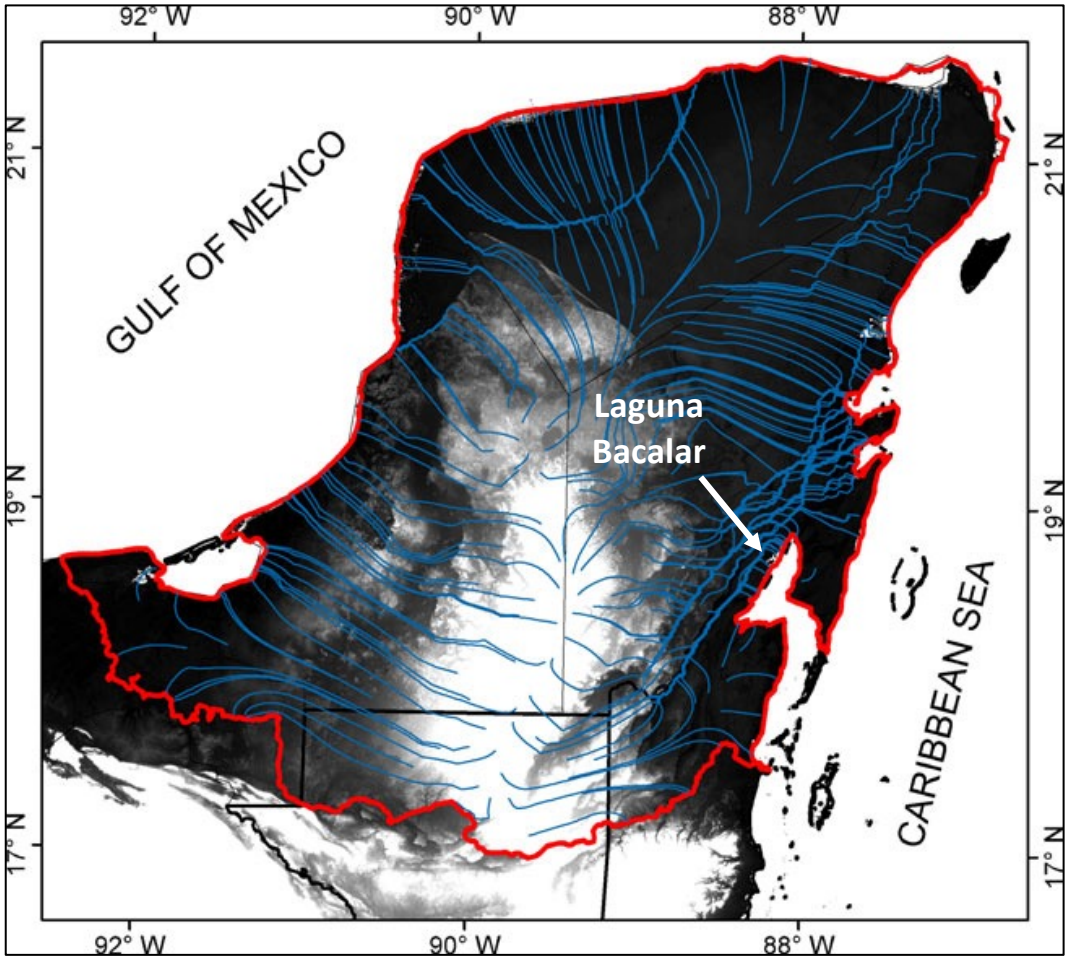

Figure 2. Yucatan Peninsula land surface elevation overlaid with groundwater streamlines. Bauer-Gottwein et al. 2011.

This study is based entirely in and around the Laguna Bacalar region of Quintana Roo, Mexico on the Yucatan Peninsula. Sampling locations range across the entire lake, various cenotes, an inland well, and surface water conduits attached to the lake. Figure 3 shows various sampling locations from 2014, 2017, 2018, and 2019. The city of Bacalar sits to the west of the lake and was the primary headquarters for field research during these sampling years. Laguna Bacalar is a marl lake, meaning it is precipitating massive amounts of calcite onto the lakebed. The clear groundwater supplied to the lake provides ample view of the rich, white calcite

sediment on the lakebed. In many areas, the sediment more closely resembles a gooey mud than a granular sand and walking on the lakebed in shallow areas is often a significant challenge.

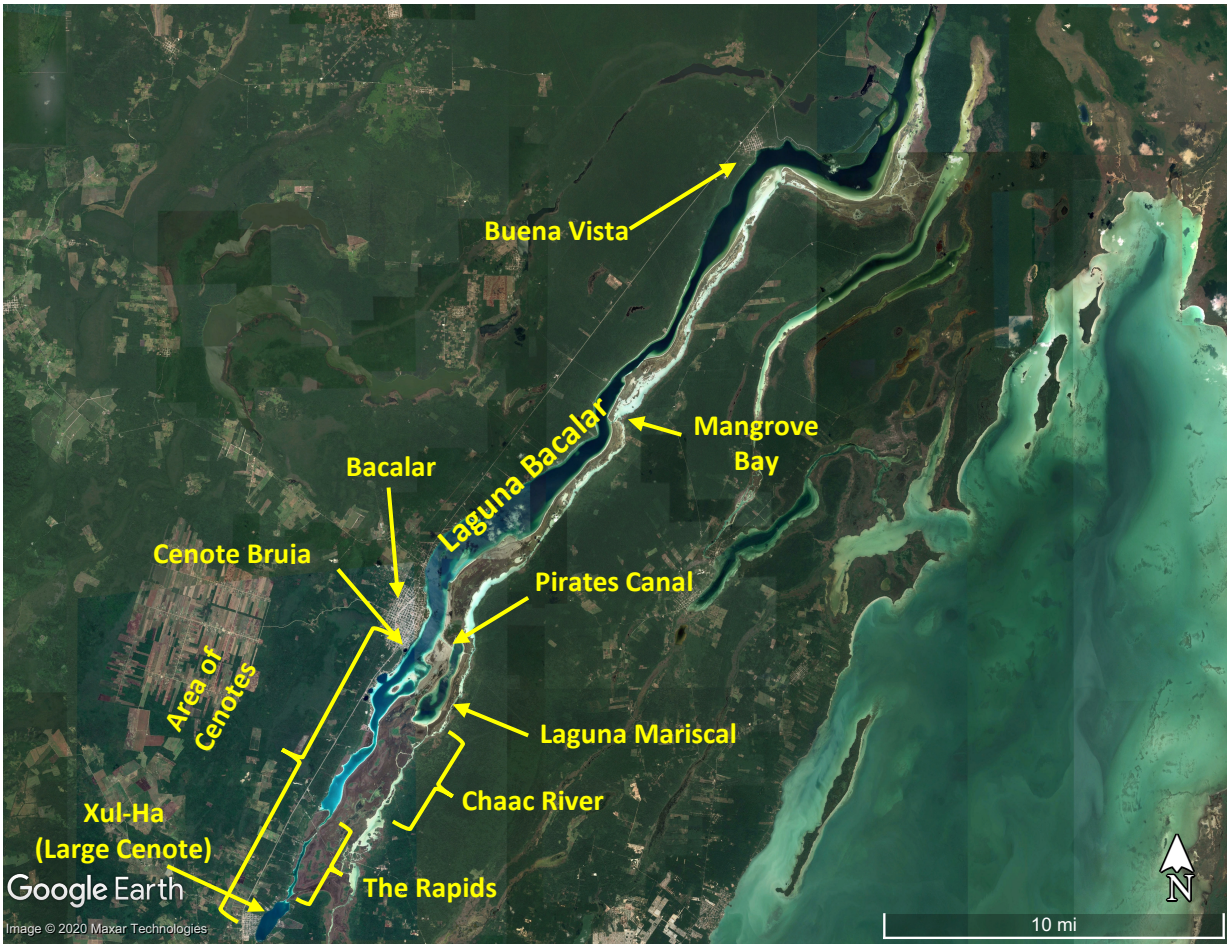

Figure 3. Points of interest in the Laguna Bacalar region.

4. Previous Research

Very little research pertaining to the hydrology of Laguna Bacalar can be found in the literature. Unpublished data has been collected by UW-Milwaukee researchers in Bacalar and the surrounding area from 2017 to 2019. Data includes $\delta^{13}C$, $\delta^{18}O$ and $\delta^{2}H$ isotopes, major ion

water chemistry, and physical flow measurements. Limited water isotope data was also collected in 2014.

The overall conceptual picture of the physical hydrology for this region points to groundwater entering into the surface water system from a region referred to as Xul Ha at the southern end of the lake and traveling northeast through the lake while receiving further groundwater input from cenotes dotting the shoreline. At this point some surface water becomes relatively stagnant and is subjected to evaporative processes in the portion of the lake north of the Pirates Canal, later referred to as Zone 3, while a large amount of water exits the lake system and flows down the Chaac River. Chemically, this lake is precipitating calcite due to an influx of CO_2 to the lake supplied by groundwater entering the system through fractures and cenotes along the shoreline. This paper will further develop these ideas.

5. Research Objectives

The overarching objective of this project is to identify and understand the physical and chemical hydrology of Laguna Bacalar using data collected on the physical flow to and from the lake, isotopes measurements of $\delta^{13}C$, $\delta^{18}O$, and $\delta^{2}H$, and major ion chemistry. This project will coalesce and quantitively interpret this previously unstudied dataset.

Based on previous research, the following hypotheses were formed regarding major ion trends and geochemical modeling, water isotopes, and carbon isotopes, and physical flow dynamics.

- The bulk groundwater inflow is entering from the southern end of the lake known as Xul Ha and is supplemented by additional water entering the lake from cenotes located farther north.
- The water at the north end of the lake has a negligible inflow/outflow and the predominant process in this area is evaporation.
- Laguna Bacalar is precipitating large amounts of calcite as is evident from hydrochemical analyses and lakebed sampling.
- Lake water has a variable residence time as evident from flow data.

The following methods were used to verify and quantify these hypotheses.

- The program PHREEQC has been used to determine the hydrochemical saturation indices of the lake (Parkhurst and Appelo 2013).
- A better understanding of evaporation signals and flow dynamics throughout the lake has emerged by analyzing the major ion's in the lake system.
- Water isotope analysis, the MM5 weather model, and data on inflow and outflow have been used in determining flow characteristics and residence time of waters in different sections of the lake system (UCAR 2003).
- Carbon isotopes have been collected to approach a better understanding of lake CO_2 evolution, calcite precipitation, and identification of CO_2 sources and sinks.

Previous research on water isotopes can assist in predicting the types of values expected to be seen in an environment like Laguna Bacalar. Both hydrogen and oxygen isotopes are measured in per mil (‰) using the Vienna Standard Mean Ocean Water (VSMOW) isotopic

standard. A range of typical oxygen and hydrogen isotope values for different natural media is displayed in Figures 4 and 5 (Kumar 2018). Laguna Bacalar is recharged from meteorically derived groundwater, so $\delta^{18}O_{VSMOW}$ and $\delta^{2}H_{VSMOW}$ values are expected to correlate with the boundaries of (sub) tropical precipitation on these figures. $\delta^{18}O_{VSMOW}$ typically ranges between approximately -2‰ and -8‰ while $\delta^{2}H_{VSMOW}$ ranges from -20‰ and -50‰ for areas receiving sub-tropical precipitation like Laguna Bacalar (Kumar 2018). This topic is expanded upon in Section 7.8, "Hydrocalculator and Meteoric Waters".

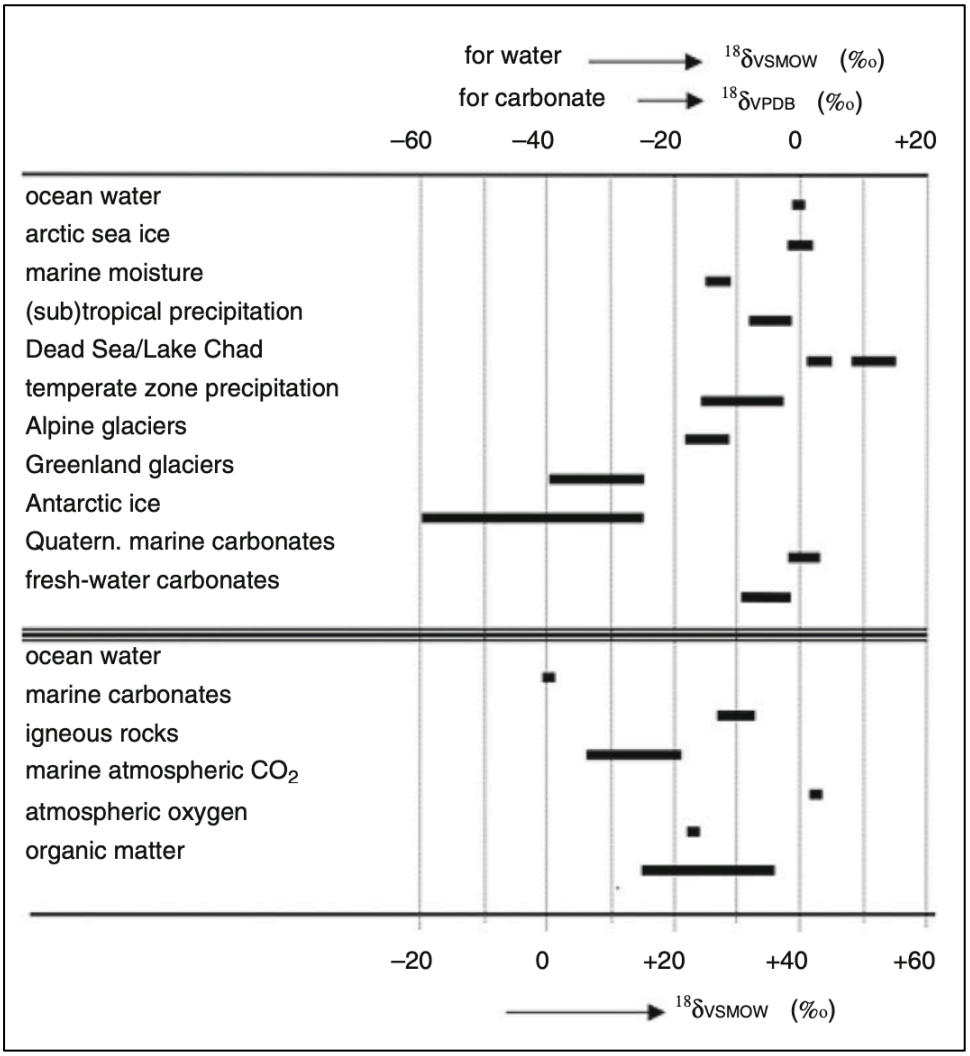

Figure 4. Range of $\delta^{18}O$ ($‰_{VSMOW}$) in natural media. Kumar 2018.

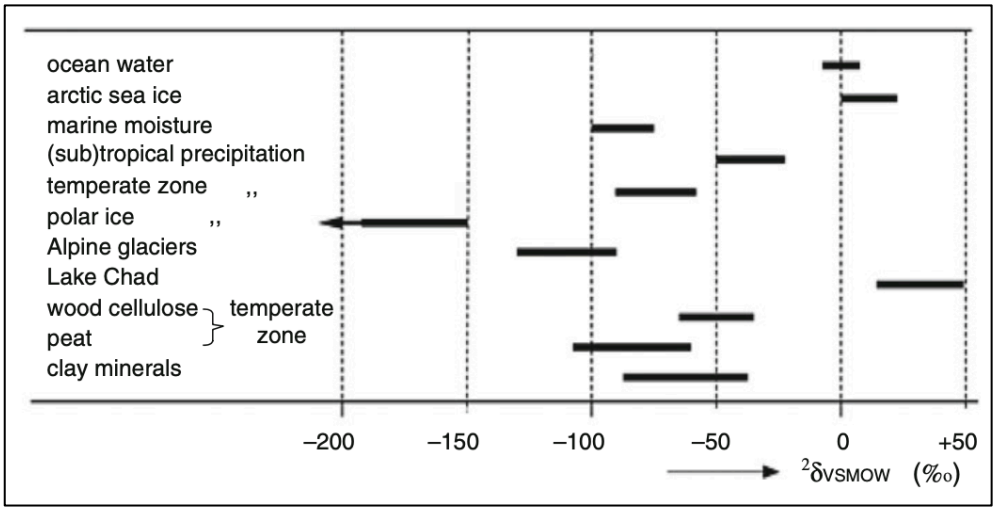

Figure 5. Range of δ^2H ($‰_{VSMOW}$) in natural media. Kumar 2018.

$\delta^{18}O_{VSMOW}$ and δ^2H_{VSMOW} data can be compared to the Global Meteoric Water Line (GMWL) in order to understand the impacts of hydrological processes on a body of water. The GMWL has a slope of 8. Figure 6 illustrates the position of theoretical meteoric water lines (MWL's) based on variations in isotopic composition of water brought on by geographical and meteorological variables including evaporation, latitude, altitude, distance from coastlines, humidity, seasonality, and more (SAHRA 2005). Laguna Bacalar is subject to significant evaporative processes that cause a depletion of light isotopes and is in an area with high relative humidity. Based on these parameters, a slope of around 5 could be anticipated for the local evaporation line (LEL) derived from Laguna Bacalar water samples (SAHRA 2005, Mook 2006, Clark and Fritz 1997).

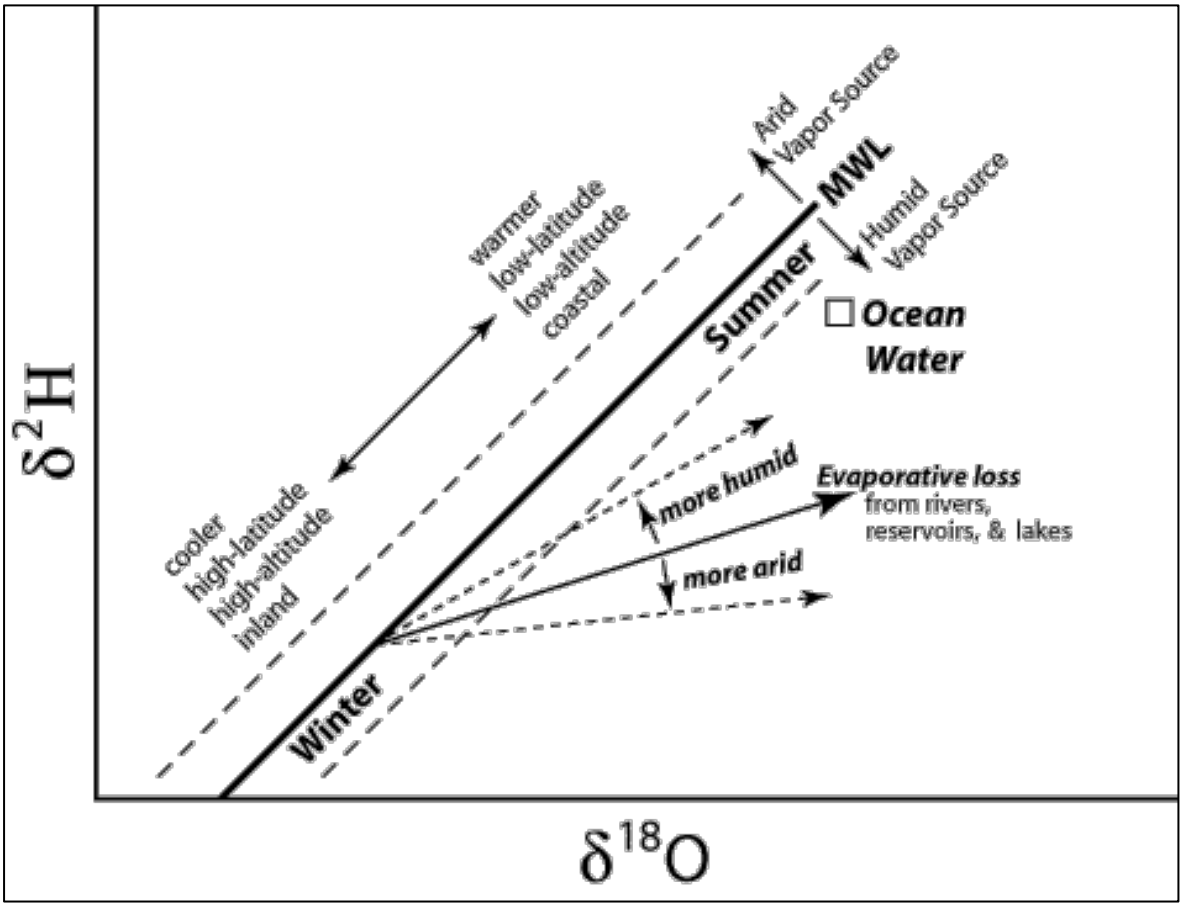

Figure 6. Variations in isotopic composition of water as impacted by hydrologic processes. SAHRA 2005.

Carbon isotope values are measured in per mil (‰) using the isotopic standard Vienna Pee Dee Belemnite (VPDB). These isotopes can assist in determining carbon sources and sinks. A general range of carbon isotopes in natural compounds is displayed in Figure 7 (Clark and Fritz 1997). The carbon isotope values expected in Laguna Bacalar groundwater is -21‰$_{VPDB}$ to -1‰$_{VPDB}$.

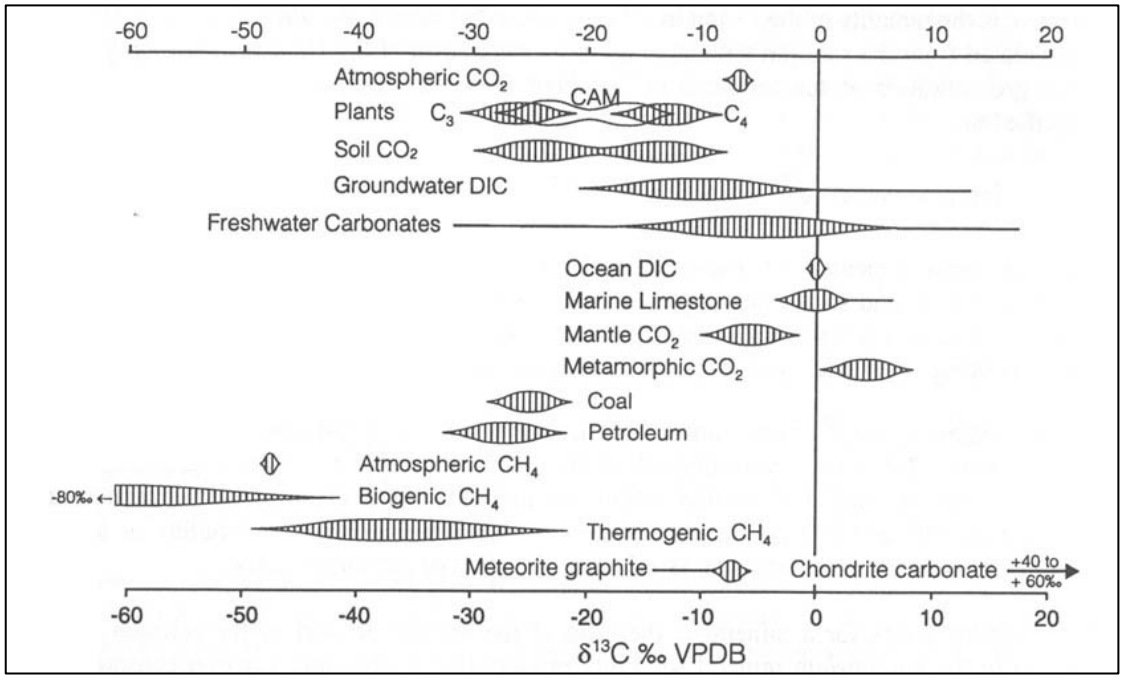

Figure 7. Range of $\delta^{13}C$ ($‰_{VPDB}$) in different natural compounds. Clark and Fritz 1997.

Figure 8 displays hydraulic conductivity measurements of various different types of rock (Heath 1983). The range of hydraulic conductivity measured in areas composed of karst bedrock extends over multiple orders of magnitude, as carbonate areas can allow water to travel through massive conduit channels such as caves and cenotes measured on the scale of meters as well as through micrometer scale matrix-level movement. When applied to Laguna Bacalar, this wide range of hydraulic conductivity values suggests water could be entering the lake system through both massive conduit passages such as cenotes and through matrix-level diffusion such as groundwater recharge of meteoric waters through the bedrock, both of which are confirmed and elaborated upon from research and data later on in this paper.

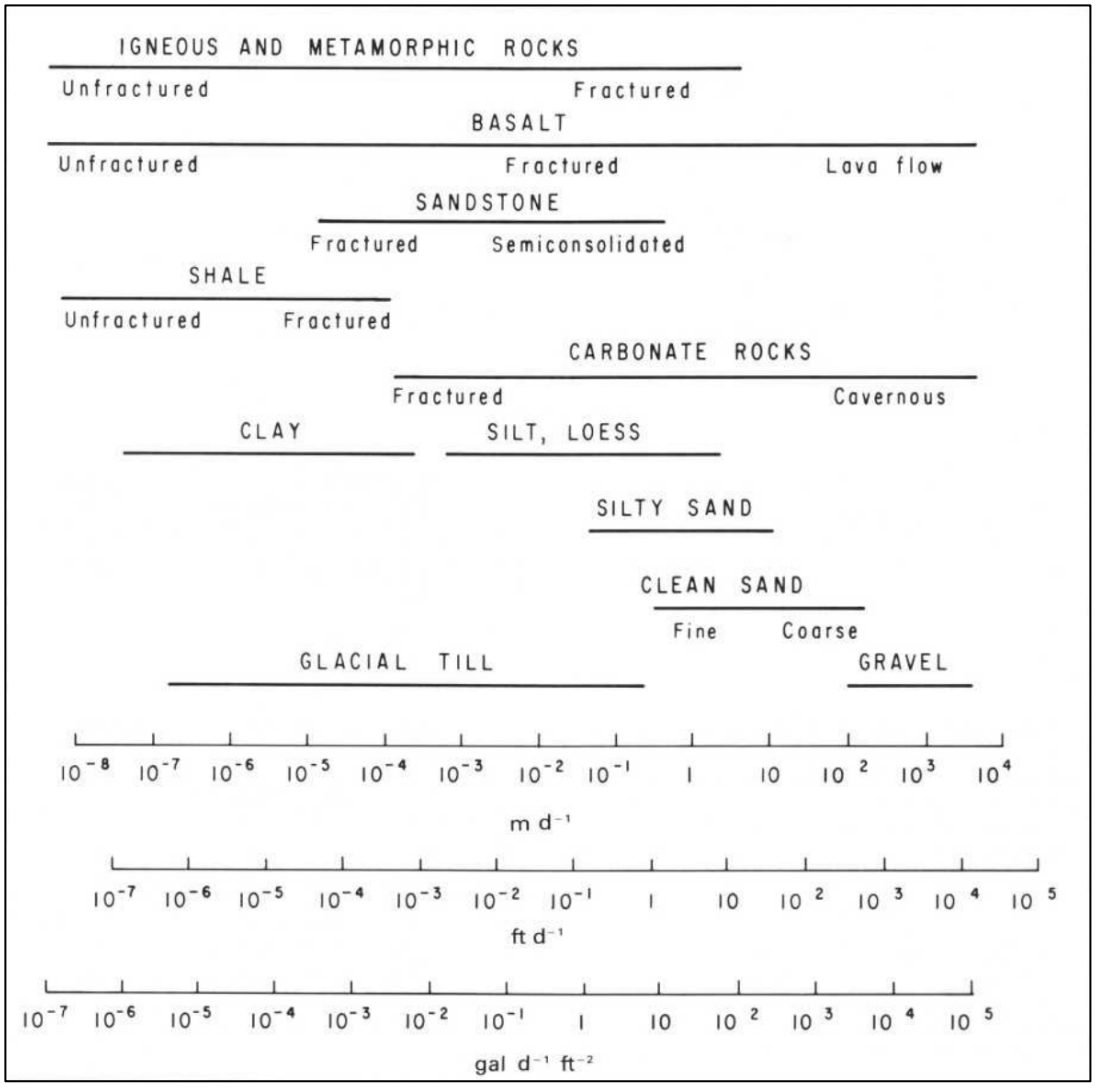

Figure 8. Hydraulic conductivity of various rock media. Heath 1983.

6. Sampling and Methods

Four different types of physical samples were collected for this project: Cations, anions, water isotopes, carbon isotopes. Sampling occurred both in the field in Laguna Bacalar and back in laboratories at UW-Milwaukee for samples obtained from 2017 to 2019. Physical data for these years was also collected from the stream gauging of two rivers in the lake system.

6.1 Major Ions and Alkalinity

Cation and anion water samples were collected at each sampling site using capped test tubes. Each test tube was filled with 10mL of water from per sampling site. Upon collection, 0.5mL of HNO_3 trace metal solution was added to each of cation test tubes exclusively. HNO_3 was added to the solution to minimize metal cation precipitation and adsorption during transport. Immediately after water samples were collected for cations and anions, a 10mL water sample was analyzed for pH using a probe calibrated with commercial buffers at pH values of 4 and 7 and a HCl titrant measured in normality, N. Sample alkalinity was calculated using Equation 1.

$$Alk_o = \frac{(1000)(B)(C_a)}{V_o} \qquad \text{EQ. 1}$$

In this equation, Alk_o is the alkalinity of the sample in meq/L, B is the volume of titrant needed to reach the HCO_3^- equivalence point, C_a is the normality of the titrant in eq/L, and V_o is the initial volume of the water sample (USGS 2013).

Lab analysis for cations was performed using a flame atomic absorption spectrometer (AA) following EPA Methods 7140, 7450, 7610, and 7770 for calcium, magnesium, potassium, and sodium, respectively (US EPA 1986). These EPA Methods are located in Appendix A. Cations analyzed were calcium, magnesium, potassium, and sodium. Ca and Mg samples were analyzed using the same standard as one another and were diluted with E-pure water and lanthanum. Na samples were diluted with E-pure water and K samples were diluted with E-pure water and cesium chloride. Data tables of cation analysis are located in Appendix B.

Lab analysis of anions was performed using an ion chromatograph (IC) following US EPA Method 300.0 (US EPA 1993). All anions were diluted in the lab at a ratio of 0.5mL of sample

and 4.5mL of E-pure water. Anions analyzed were chloride, sulfate, phosphate, and nitrate. Bicarbonate content of these samples was calculated by balancing cations and anions. Data tables of anion analysis are located in Appendix B.

6.2 Water Isotopes

Water isotope data is a measure of $\delta^{18}O$ and $\delta^{2}H$. $\delta^{18}O$ refers to a measure of the ratio of stable isotopes ^{18}O:^{16}O. $\delta^{2}H$ is the measure of stable hydrogen isotopes ^{2}H:^{1}H. Equations defining the measure of $\delta^{18}O$ and $\delta^{2}H$ are defined in Equation 2 and Equation 3, respectively.

$$\delta^{18}O = \left(\frac{\left(\frac{^{18}O}{^{16}O}\right)sample}{\left(\frac{^{18}O}{^{16}O}\right)standard} - 1 \right) \times 1000‰ \quad \text{EQ. 2}$$

$$\delta^{2}H = \left(\frac{\left(\frac{^{2}H}{^{1}H}\right)sample}{\left(\frac{^{2}H}{^{1}H}\right)standard} - 1 \right) \times 1000‰ \quad \text{EQ. 3}$$

Sampling of water isotopes was similar to that of anions and alkalinity. Collection of these samples consisted of filling a sampling container and sealing it with no headspace. This is the only step prior to shipping samples to the laboratory for testing. This follows the guidelines outlined in Groundwater Sampling Procedures for Isotope Hydrology (International Atomic Energy Association 2014). Samples in this project were tested at the Environmental Isotope Laboratory within the Geosciences Department at University of Arizona. Data tables of water isotope analysis are located in Appendix B.

6.3 Carbon Isotopes

Carbon isotope samples were collected at many of the same sites as water isotope samples. Similar to water isotopes, carbon isotope delta values, referred to as $\delta^{13}C$, are a measure of the ratio of stable isotopes ^{13}C:^{12}C. Equation 4 defines the measure of $\delta^{13}C$.

$$\delta^{13}C = \left(\frac{\left(\frac{^{13}C}{^{12}C}\right)sample}{\left(\frac{^{13}C}{^{12}C}\right)standard} - 1 \right) \times 1000‰ \qquad \text{EQ. 4}$$

Carbon isotope sampling procedures followed a variation of the guidelines published in Groundwater Sampling Procedures for Isotope Hydrology (International Atomic Energy Association 2014). Sampling was performed through the following steps:

- Water samples were collected in plastic bottles.
- Pellets of NaOH were added to each bottle to raise the pH of the samples to at least 9.
- $BaCl_2$ was added to the bottles and shaken vigorously for the purpose of converting all carbonate species to CO_3^{2-} for carbon isotope collection.
- After cloudiness of water subsided, carbonate precipitant accumulated on the bottom of containers.
- Additional $BaCl_2$ was added to the bottles to ensure complete precipitation had occurred.
- Water bottles were slowly decanted to leave only the precipitant.
- Carbon isotope samples were transported to UW-Milwaukee for analysis in the isotopic lab at the School of Freshwater Sciences.

Data tables of carbon isotope analysis are located in Appendix B.

6.4 Stream Gauging

Stream gauging of two areas of the Laguna Bacalar system was performed for all three years. Stream gauging data was gathered following the midsection method guidelines (World Meteorological Organization 2010). A diagram of this method is shown in Figure 9. The midsection method of stream gauging is performed using a current meter and measuring the depth and velocity of cross-sectional segments of a stream. Gauging was performed as follows:

- Researchers chose a segment of each river and measured the width using a measuring tape.
- Researchers sectioned the Rapids into 11 segments and the Chaac River into 18 segments approximately 2m apart each.
- Velocity measurements were taken at each segment at 2/3 of the total depth below the water surface using a current meter.
- Total discharge in each segment was calculated using Equation 5,

$$q_n = v_n \left[\frac{b_n - b_{(n-1)}}{2}\right] d_n \qquad \text{EQ. 5}$$

  where q_n is the partial discharge through a segment, v_n is the velocity of water through a segment, b_n is the distance from the initial segment, $b_{(n-1)}$ is the distance from the initial segment to the preceding segment, and d_n is the depth of water at the segment measured.
- All of the q values were averaged, and total flow velocities were derived for each site.

Calculations of the Chaac River and the Rapids are located in Appendix B.

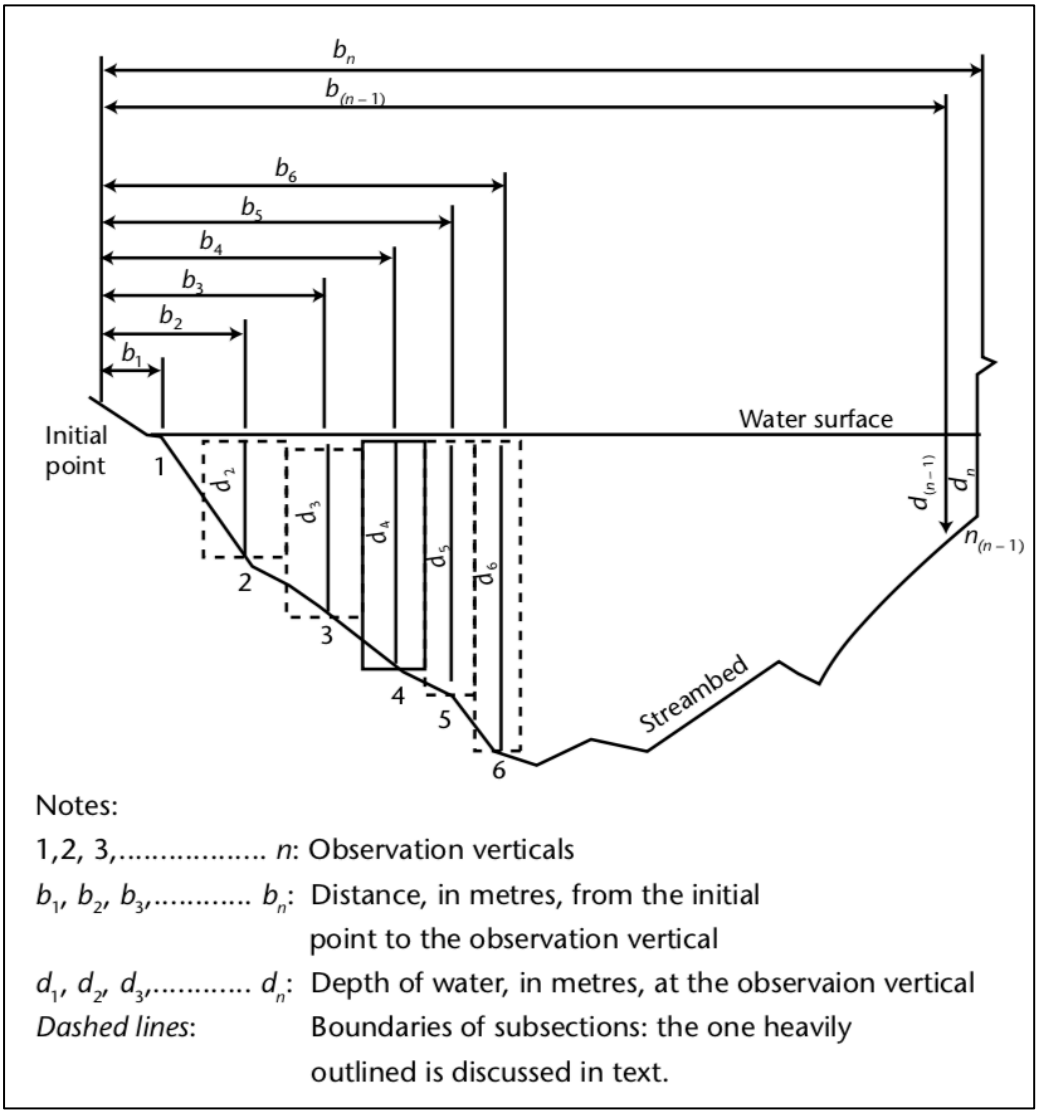

Figure 9. Midsection method of computing cross-section area for discharge measurements. World Meteorological Organization 2010.

6.5 Sediment Collection and Analysis

During the 2019 sampling trip, one lakebed sediment sample was collected along with three sediment cores derived from stromatolites within the lake. A previous XRD lab analysis of sediment samples indicated that the local calcite bedrock and calcite precipitating from Laguna Bacalar waters is composed of approximately 3% Mg substitution for Ca in the calcite chemical structure. The sediment samples collected in 2019 were brought back to the lab and used to

determine the ratio of calcium to magnesium in the calcite-rich sediment of the lake and analyzed through the following procedure.

- Sediment was dried and a small amount was weighed and placed into individual test tubes.
- Sediment was dissolved using a ratio of 4mL of deionized water and 1.1mL of a HCl solution previously diluted 4:1.
- Samples were centrifuged and filtered to remove any non-calcite particulate matter.
- Solutions were analyzed using US EPA Methods 7140 for Ca and 7450 for Mg on an AA (US EPA 1986).

Sediment sampling locations from 2019 are shown in Figure 10. XRD and AA analysis results are provided in Appendix B.

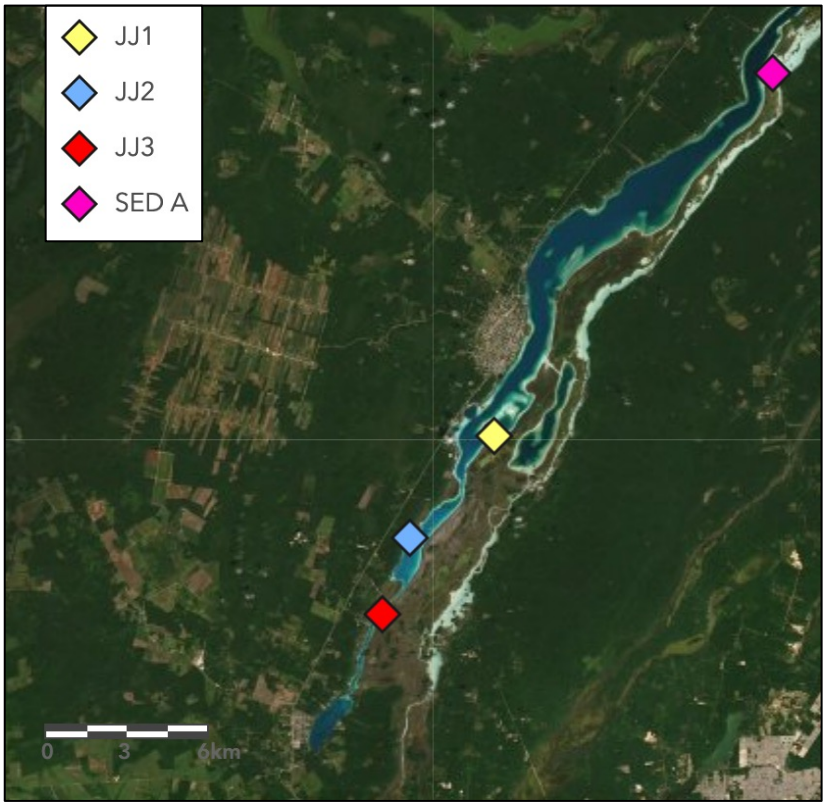

Figure 10. Lakebed sediment core and oncoid core sampling locations.

7. Results

7.1 Sediment Analysis

AA analysis on the calcite sediments revealed that the ratio of calcium to magnesium ranged from 26.5:1 to 36.9:1. This data was used to yield more specific ion speciation results in the program PHREEQC (Parkhurst and Appelo 2013). This also indicates that the calcite precipitant in the lake is not undergoing overly significant ion substitution of Mg for Ca. PHREEQC ion speciation data is expanded upon in Section 7.9 “Major Ions and Saturation Indices”.

7.2 Stream Gauging Results

Stream gauging was performed at the sole surface water inlet and outlet locations of Laguna Bacalar. The inlet is referred to as the Rapids. The Chaac River lies to the east of Laguna Bacalar and serves as the sole surface water outlet. These two locations were gauged annually from 2017 to 2019 in the month of January. As indicated in Figure 11, the flow volume fluctuates from year to year but the annual difference in flow between the Rapids and Chaac River remains overall constant. The locations of these two areas are indicated in Figure 3.

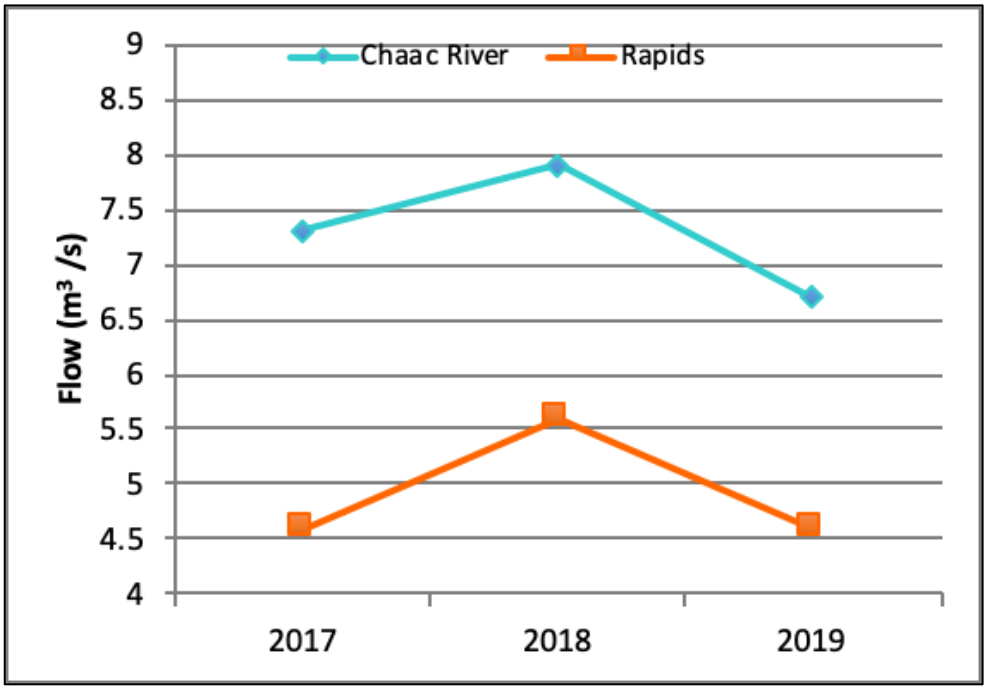

Figure 11. Flow comparison in two stream gauged sites.

Year	Rapids (m^3/sec)	Chaac (m^3/sec)	Additional Flow out of Chaac River (%)	Rapids:Chaac Ratio (%)
2017	4.6	7.3	37.0	63.0
2018	5.6	7.9	29.1	70.9
2019	4.6	6.7	31.3	68.7

Table 1. Flow comparison of two stream gauged sites.

Figure 12 is a base map of the Laguna Bacalar region overlain with a hypothetical precipitation catchment area. This represents the surface area necessary to supply the annual amount of 2016 rainfall needed to match the outflow gauged through the Rapids in January 2017 for an entire year. Streams were gauged in January of each sampling year and of the three years gauging occurred 2016 was the year with the least amount of rainfall and therefore the largest catchment area. The catchment area necessary to capture the rainfall during 2016 in order to supply the flow seen in 2017 is 3.36e+08 m^2. Rainfall in 2018 was nearly twice the

amount of 2016 and 2017, which would require a catchment with a smaller surface area. For 2019 the catchment area required was less than half the size of the 2017 catchment area at 1.48e+08 m^2. Rainfall data used for this calculation was sourced from World Weather Online (2020). Rainfall capture area calculations are located in Table 2 and Appendix B.

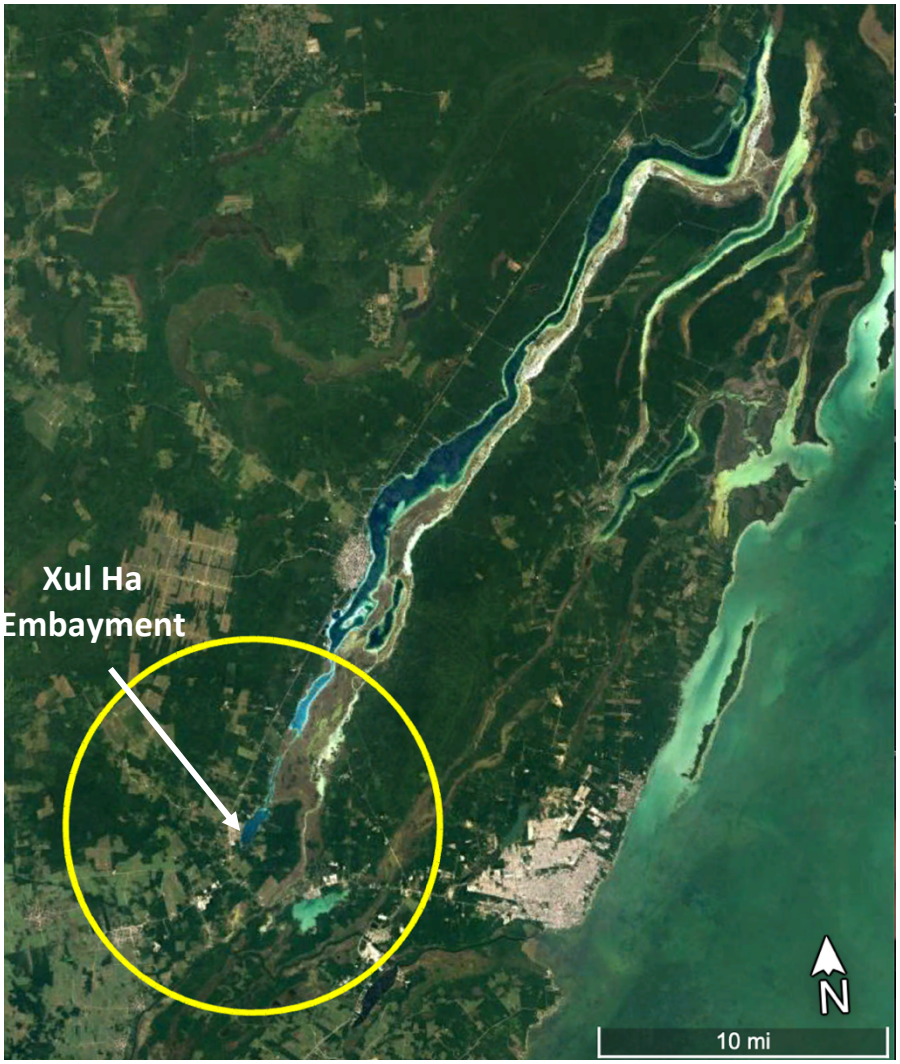

Figure 12. Hypothetical rainfall catchment area for observed January 2017 Rapids flow.

Year	Rapids Flow (m^3/yr)	Precipitation (m/yr)	Catchment Area (m^2)
2016	-	0.43	-
2017	1.45E+08	0.55	3.36E+08
2018	1.77E+08	0.98	3.23E+08
2019	1.45E+08	-	1.48E+08

Table 2. Rainfall catchment areas based on Rapids flow.

7.3 CO_2 and Alkalinity Trends

Figure 13 is a graph comparing trends of excess pCO_2 and pH of sampling sites organized from south to north, which is the general flow path in the lake system. Bars outlined in red indicate samples taken from groundwater sources, including a well, cenotes, and springs. Samples with no red outline are surface water samples within the lake. The cross-hatched bars representing the "Juan Carlos Well" sampling location in Figures 13, 14, and 15 indicates that it is the only sample obtained from a groundwater well, while the remainder of samples were taken from surface water or groundwater sources that were sampled at lake level rather than sub-lithic sampling origins.

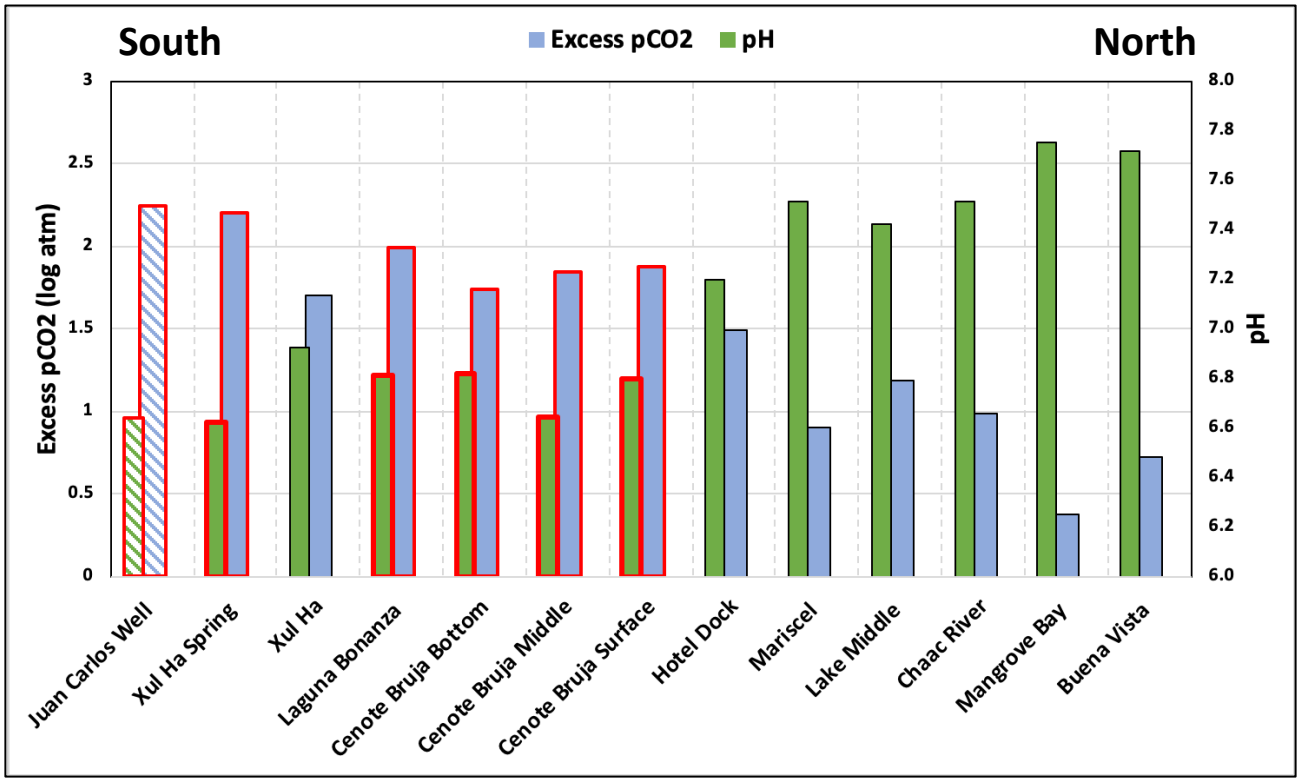

Figure 13. Excess pCO_2 and pH trends by location. Southernmost samples are on the left.

As meteoric waters infiltrate the soil zone on top of bedrock, extra CO_2 from bacterial respiration is injected into the water. The resultant groundwater then contains more CO_2 than the atmosphere. When the groundwater enters the lake this excess CO_2 exsolves from the lake in an attempt to reach equilibrium with the atmosphere. The general trend seen in Figure 13 from south to north is a decrease in CO_2 except in cenote samples. Cenote samples are richer in CO_2 than the surface water samples at Xul Ha. Cenote Bruja Bottom, Middle, and Surface have very similar levels of excess pCO_2 because these samples were all within the same column of rising cenote water. A jump in excess pCO_2 is indicated at the Lake Middle sampling site because this site is near Cenote Bruja which is mixing with surface water that has already exsolved some CO_2 heading north in the lake. None of the sampling sites are at complete equilibrium with air because of a consistent supply of groundwater moving north. Additionally, biogenic CO_2 is consistently added to the water across the entire lake system. The combined biological activity and groundwater infiltration through karst bedrock means that the lake never reaches atmospheric equilibrium with CO_2.

An inverse trend is evident for pH levels. Acidic CO_2 is constantly exsolving from the system as water moves farther from groundwater inputs. This causes pH levels to be most basic in the northern end of the lake where there is little to no addition of fresh groundwater due to the lack of cenotes.

7.4 Evaporation Signals

Figure 14 displays the chloride concentration of 2017 water samples arranged from south to north in the lake. The hatch-marked column at the Juan Carlos Well indicates that it

was the only well sample while the rest of the columns were obtained from surface water sampling methods. Chloride is significantly more concentrated in the northern end of the lake and it is a good indicator of evaporation because as water evaporates, chloride becomes more concentrated. Laguna Bacalar is a steady-state lake because it has continual inflow year-round with negligible variance in the water level, however, water heading north has longer residence times and is subject to more extensive evaporation as evident from the rising chloride concentrations.

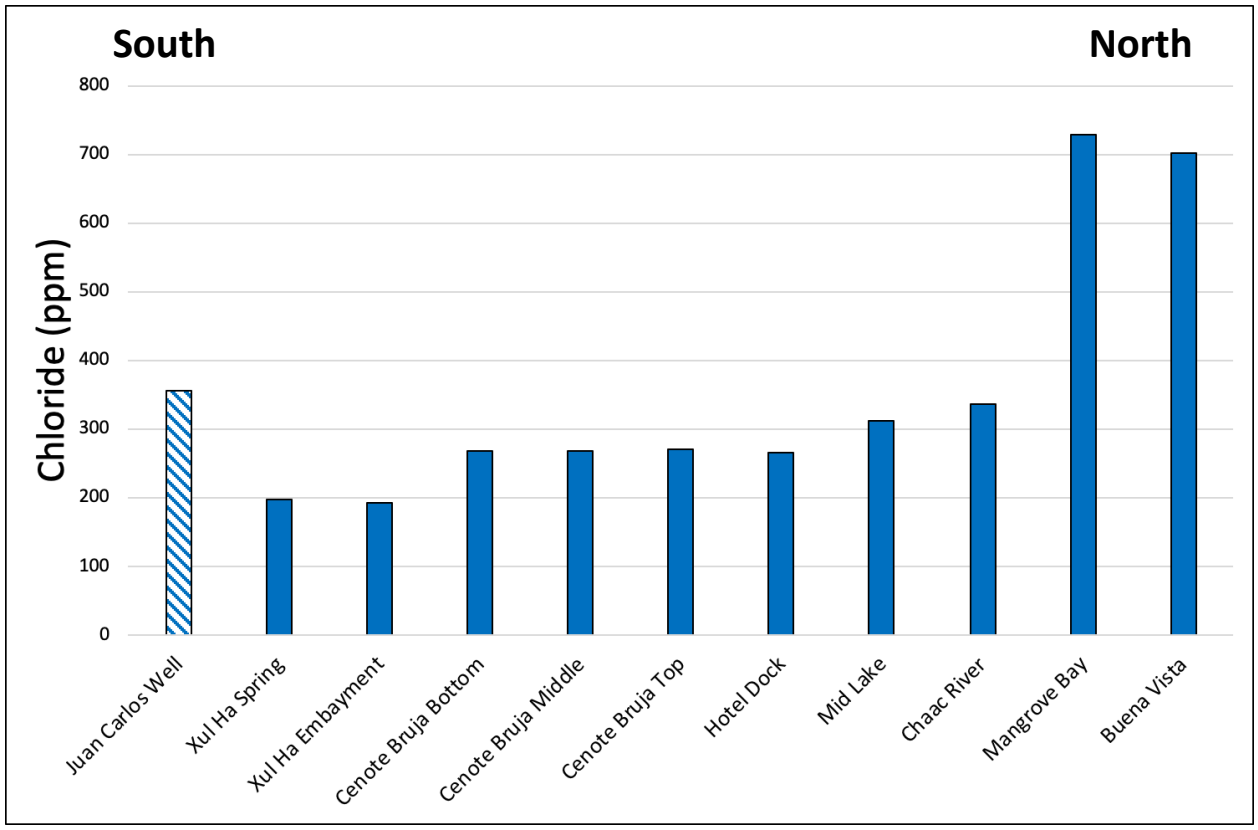

Figure 14. Chloride concentration of 2017 samples. Southernmost samples are on the left.

Figure 15 shows delta $\delta^{18}O$ arranged from south to north in the lake for the 2017 sampling year. $\delta^{18}O$ is a measure of the ratio of stable isotopes ^{18}O:^{16}O. In this case ^{18}O weighs more than ^{16}O and when surface water evaporates it preferentially evaporates lighter isotopes.

As evident in Figure 15, evaporation of lighter ^{16}O leads to the remaining surface water becoming enriched in heavier ^{18}O. This trend extends all the way north in Laguna Bacalar and indicates evaporation is a major hydrochemical process in the lake system, especially in the northern portion of the lake where no cenote inflow is present to enrich in the water in lighter ^{16}O.

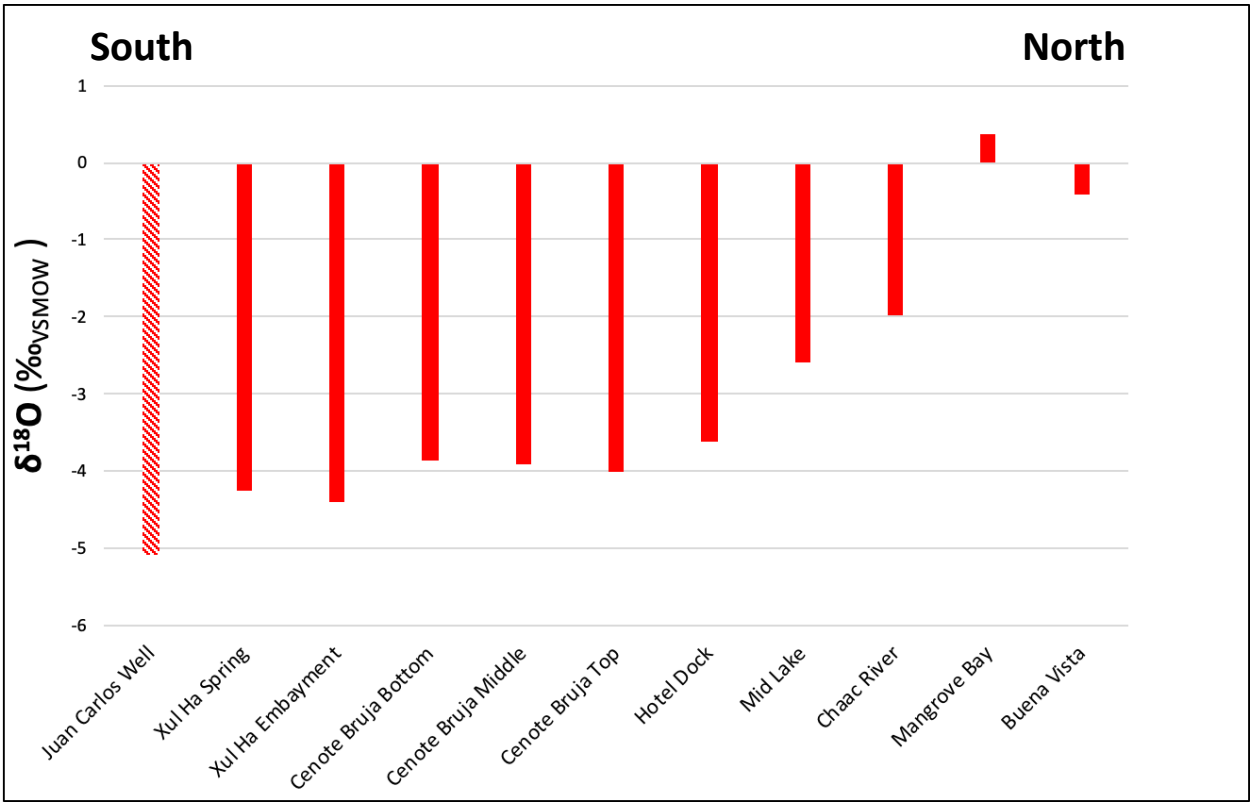

Figure 15. Light oxygen isotope depletion trend in 2017 samples. Southernmost samples are on the left.

Figure 16 is a comparison of the global meteoric water line (GMWL) to a local evaporation line (LEL) developed from data collected in the Bacalar region. The GMWL depicts the average water isotope values derived from meteoric waters globally. The sites plotted on the LEL are all categorized as surface water or groundwater including a well, cenotes, and springs. The Laguna Bacalar region is karst and all groundwater is recharged directly from

meteoric water, so as expected the groundwater samples on the LEL correlate strongly with the GMWL.

Lake water evaporation causes water isotopes to undergo Rayleigh-type non-equilibrium fractionation processes in which there is an exchange back and forth between liquid water and water vapor, though net evaporation ends up being greater than net condensation (Mook 2006). When water evaporates the lighter isotopes tend to evaporate more readily. This causes surface waters to become more enriched in heavy isotopes. The slope of evaporation lines varies based on relative humidity. Very low relative humidity values produce slopes around 4. Relative humidity values in the range of 25% to 75% will have slopes of 4 to 5. Relative humidity values of 95% or more will approach a slope of 8 and match the GMWL slope (Clark and Fritz 1997). The slope of the Laguna Bacalar LEL is 5.4 and matches observed relative humidity values which average 78%. The surface water sampling sites are enriched in heavier isotope values, which is indicative of evaporative processes (SAHRA 2005). Locations of surface water samples moving left to right on the graph are also arranged south to north, which again confirms the evaporation pattern in the lake. Groundwater samples on this graph were collected from cenotes and at Xul Ha. These sampling sites are supplying groundwater to the lake and have not lost any water to evaporation yet.

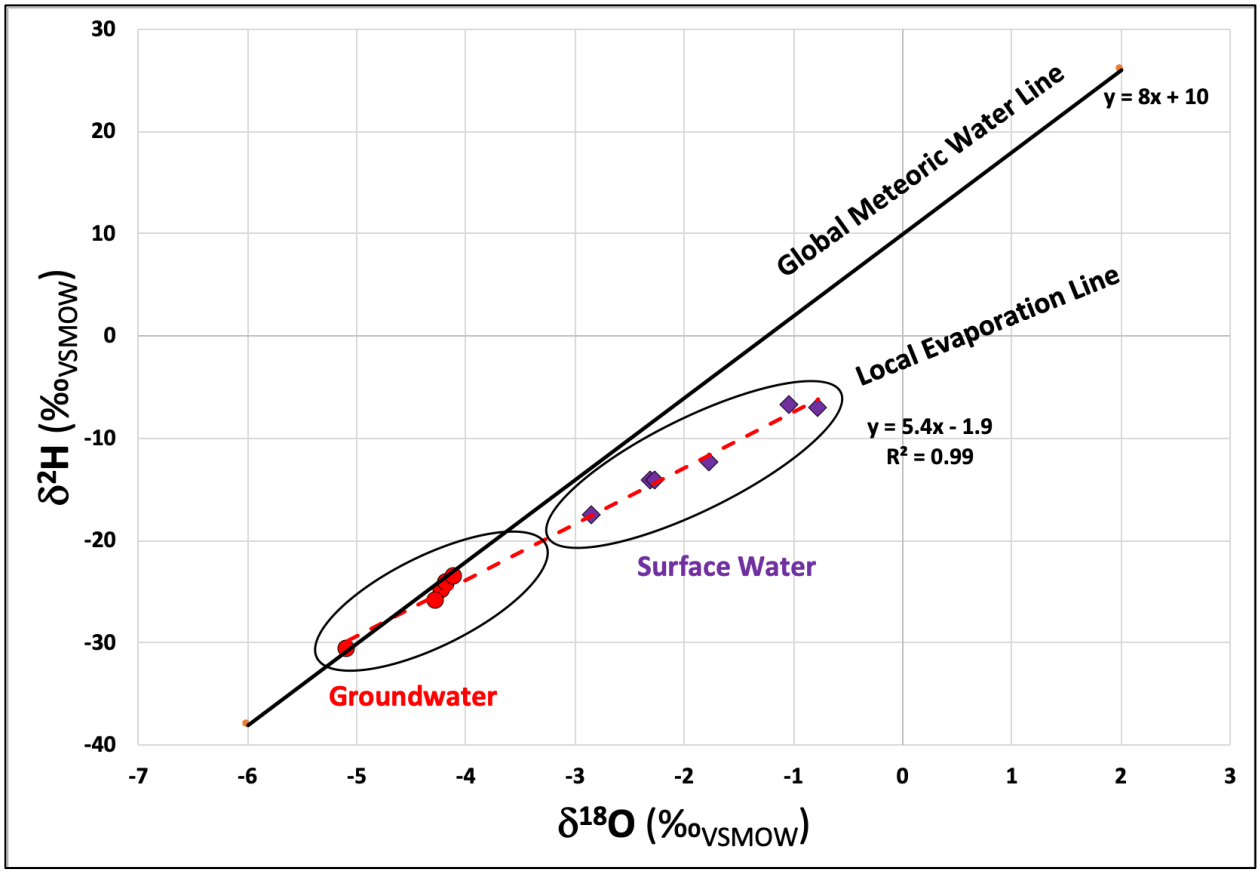

Figure 16. Global Meteoric Water Line and Laguna Bacalar Local Evaporation Line.

7.5 Cenote Inflow Contribution

Figure 17 is a map of transect pathways of sonde profile data taken from a boat in the immediate vicinity of Cenote Bruja. The location of Cenote Bruja is just south of the city of Bacalar and is noted on Figure 3. The boat track is shown entering and exiting solely across the southern entrance of the cenote. This is due to a shallow sandbar feature encompassing the top portion of the inlet that makes motorboat travel cumbersome. Sampling was performed using a sonde profiler in order to determine if there was water contribution to the greater lake system. Data the sonde collected includes temperature, pH, specific conductivity, and dissolved oxygen. Figures 18a-d display the results of this data.

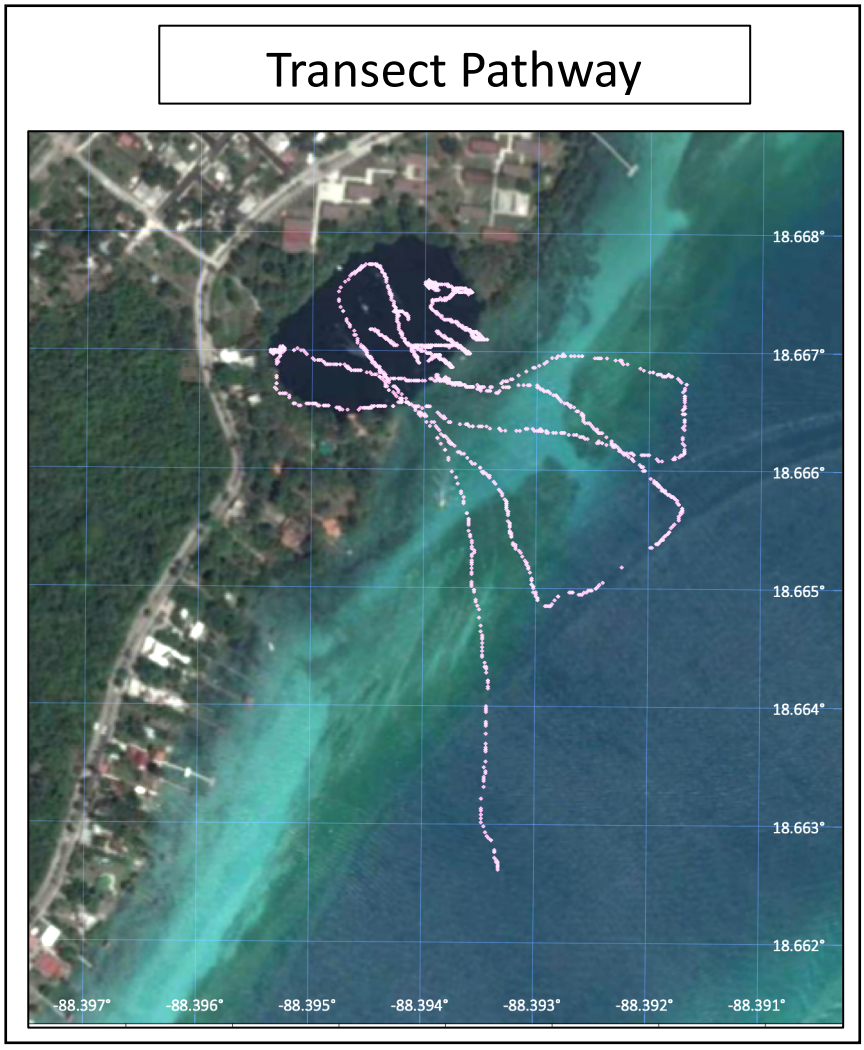

Figure 17. Cenote Bruja sonde transect pathway. Mapping is courtesy of Jessie Grow, UW-Milwaukee School of Freshwater Sciences.

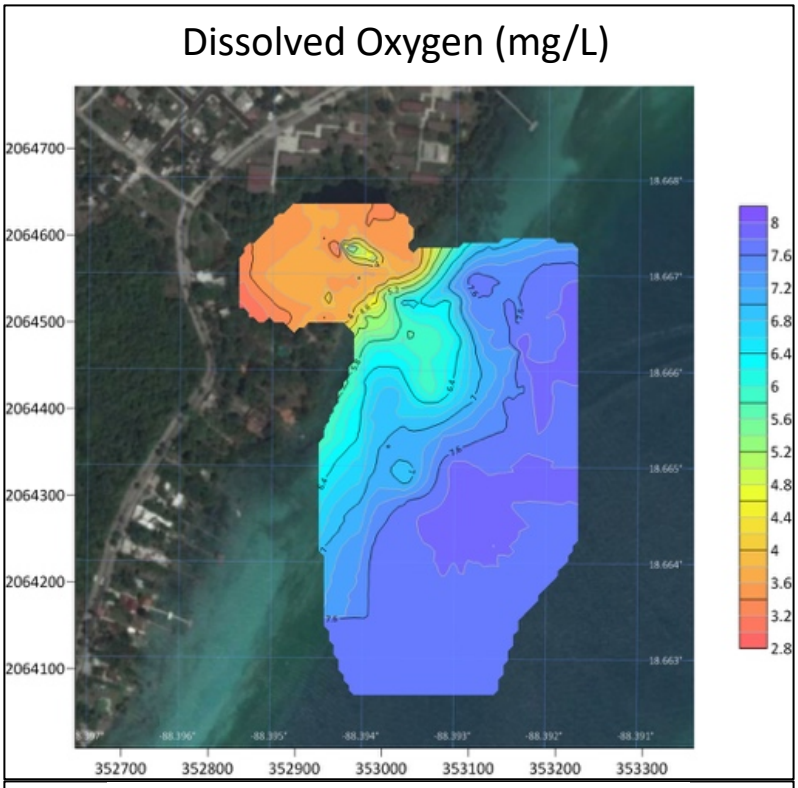
Dissolved Oxygen (mg/L)
2064700
2064600
2064500
2064400
2064300
2064200
2064100
352700
352800
352900
353000
353100
353200
353300
8
7.6
7.2
6.8
6.4
6
5.6
5.2
4.8
4.4
4
3.6
3.2
2.8

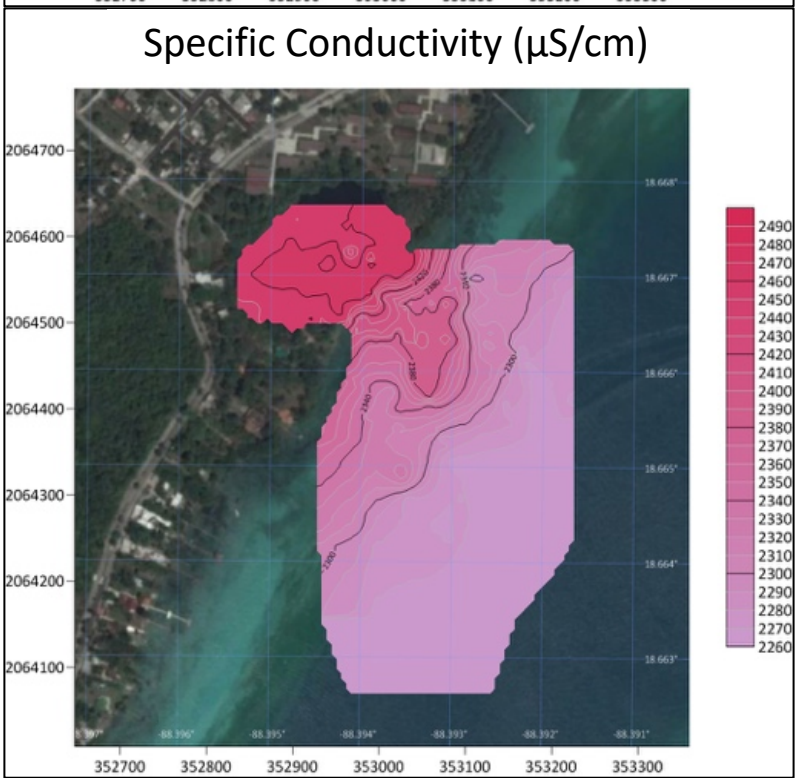
Specific Conductivity (µS/cm)
2064700
2064600
2064500
2064400
2064300
2064200
2064100
352700
352800
352900
353000
353100
353200
353300
2490
2480
2470
2460
2450
2440
2430
2420
2410
2400
2390
2380
2370
2360
2350
2340
2330
2320
2310
2300
2290
2280
2270
2260

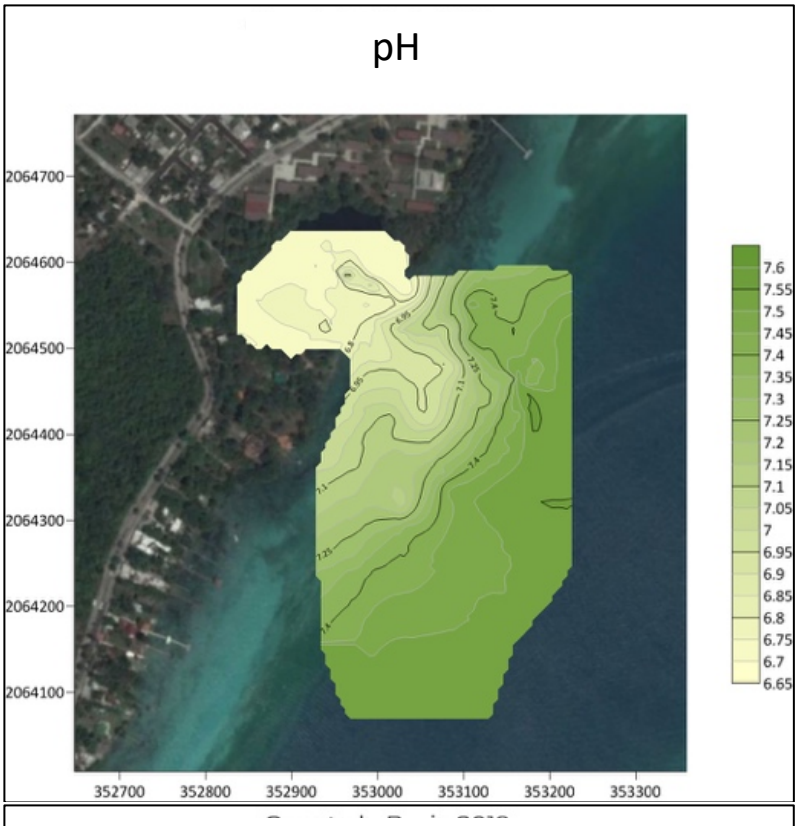
pH
2064700
2064600
2064500
2064400
2064300
2064200
2064100
352700
352800
352900
353000
353100
353200
353300
7.6
7.55
7.5
7.45
7.4
7.35
7.3
7.25
7.2
7.15
7.1
7.05
7
6.95
6.9
6.85
6.8
6.75
6.7
6.65

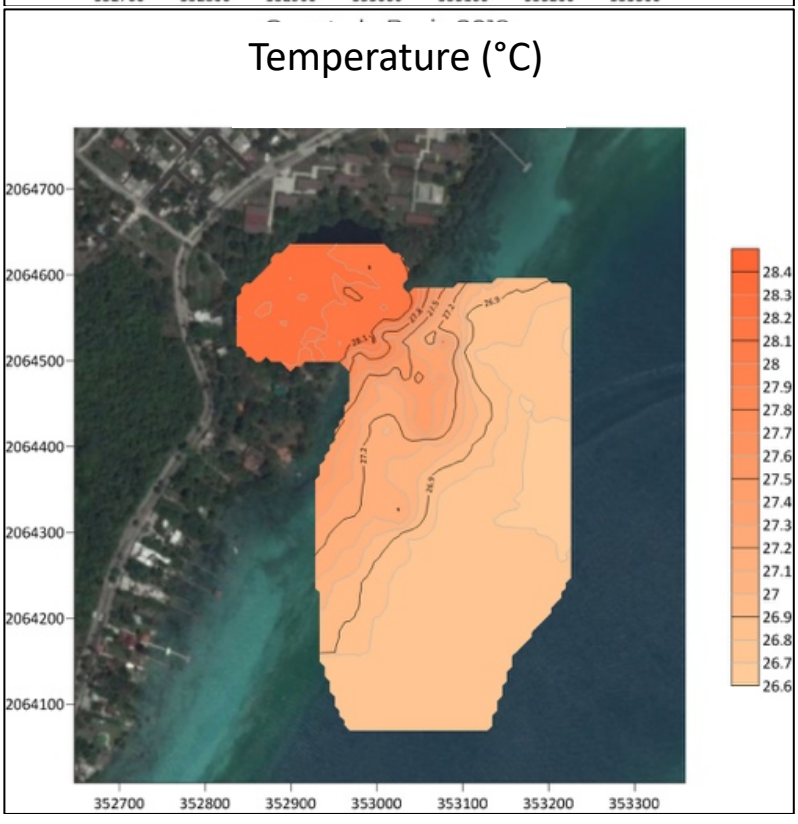
Temperature (°C)
2064700
2064600
2064500
2064400
2064300
2064200
2064100
352700
352800
352900
353000
353100
353200
353300
28.4
28.3
28.2
28.1
28
27.9
27.8
27.7
27.6
27.5
27.4
27.3
27.2
27.1
27
26.9
26.8
26.7
26.6

Figures 18a-d. Cenote Bruja groundwater plume diagrams of Dissolved Oxygen, Specific Conductivity, pH, and Temperature, respectively. Mapping is courtesy of Jessie Grow, UW-Milwaukee School of Freshwater Sciences.

As expected for a cenote discharging groundwater, Figure 18a illustrates an increase in DO as the water exits the cenote and the water becomes more oxygenated due to exposure to the atmosphere. Figure 18b shows a drop in specific conductivity as the groundwater becomes more diluted entering the lake. Figure 18c indicates that pH rises as CO_2 is lost upon reaching the water surface and entering the lake. Figure 18d illustrates a decline in temperature as groundwater enters the lake. Groundwater temperatures stay relatively consistent year-round, whereas the lake is cooler during the winter months. Figures 18a-d indicate that groundwater is entering into Laguna Bacalar through Cenote Bruja. The same situation is likely occurring in the other shoreline cenotes.

7.6 Quantification of CO_2 Exsolved and Calcite Precipitation

Figure 19 is a graph comparing the mass of CO_2 exsolved from surface water in Xul Ha Spring and Xul Ha Bay. Xul Ha Bay is a large cenote that is recharged solely via groundwater influx. The Xul Ha Bay sampling site is in the approximate center of the cenote. The water coming out of Xul Ha Spring is pure groundwater that is supersaturated in CO_2 with respect to the atmosphere. The water begins exsolving CO_2 once the water contacts the atmosphere. The greater Xul Ha Bay area undergoes evaporative processes and continual exsolution of CO_2. The y-axis represents the amount of CO_2 that would need to be exsolved from Xul Ha Spring and Xul Ha Bay water in order to reach equilibrium with the atmosphere. The difference in the two

columns on this graph is the amount of CO_2 exsolved into the atmosphere in Xul Ha Bay. Assuming this is consistently maintained year-round, Xul Ha Spring exsolves CO_2 at a rate of $4.45*10^7$ kg/yr.

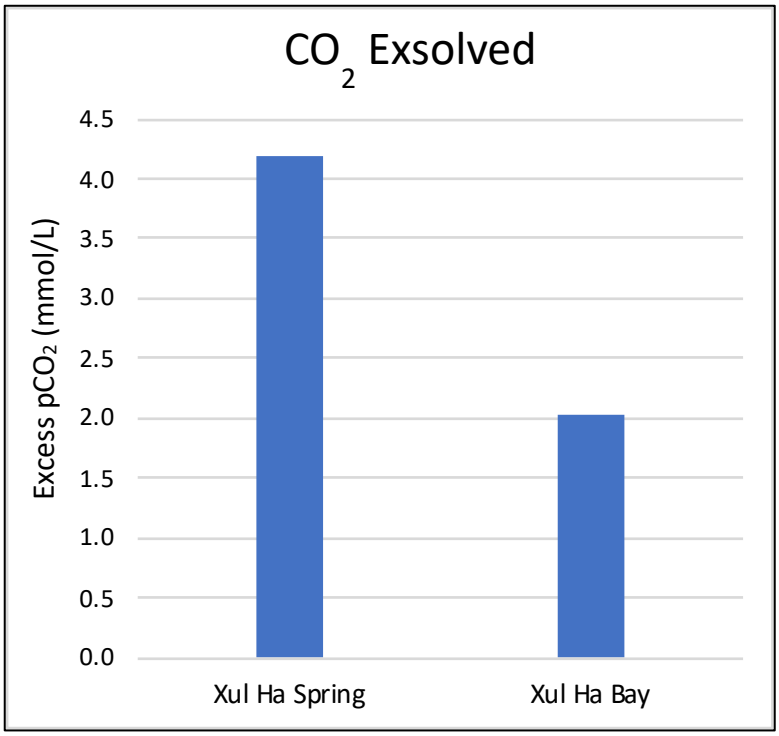

Figure 19. Amount of CO_2 above atmospheric equilibrium in Xul Ha Spring compared to Xul Ha Bay.

Similarly, Figure 20 is a graph of calcite precipitating out of the water column between Xul Ha Spring compared to Xul Ha Bay. This graph follows the same trend as Figure 19, where the y-axis is representative of the amount of calcite that would be precipitated if the reaction reached saturation with respect to calcite and the difference between the two columns is the amount of calcite precipitated in Xul Ha Bay. In an entire year, Xul Ha Spring precipitates calcite at a rate of $3.99*10^7$ kg/yr. Over the entire Xul Ha area, this equates to approximately 7.6mm of calcite annually.

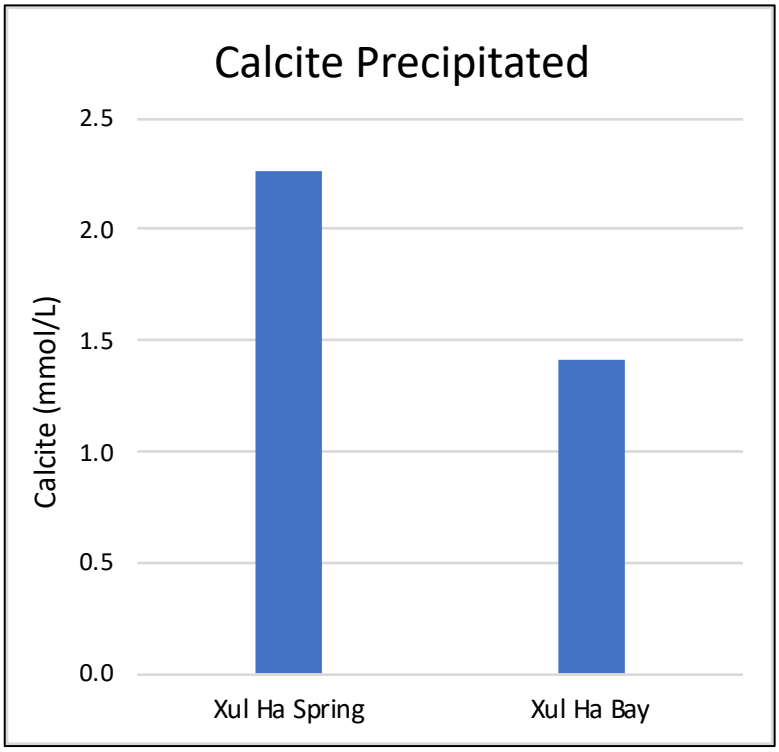

Figure 20. Amount of calcite precipitation necessary to reach equilibrium in Xul Ha Spring compared to Xul Ha Bay.

7.7 Evapotranspiration

Other factors that play a significant role in the hydrology of the lake are annual rainfall and wind. Average monthly and annual rainfall data for 2015 to 2019 is displayed in Table 3 (World Weather Online 2020). Wind in this area predominantly blows in the east-southeast direction over the course of any given year. Figure 21 shows frequency of wind annually categorized by direction (Wind History 2011).

Total Annual Precipitation (mm)			
2016	2017	2018	2019
431.71	546.45	982.84	1375.7

Average Monthly Precipitation 2016-2019 (mm)	
Jan	37.7
Feb	30.9
Mar	17.8
Apr	44.5
May	24.9
Jun	82.8
Jul	41.6
Aug	100.9
Sep	106.1
Oct	209.0
Nov	83.1
Dec	55.0

Table 3. Total annual precipitation (mm) and average monthly precipitation for 2016-2019 (mm). World Weather Online 2020.

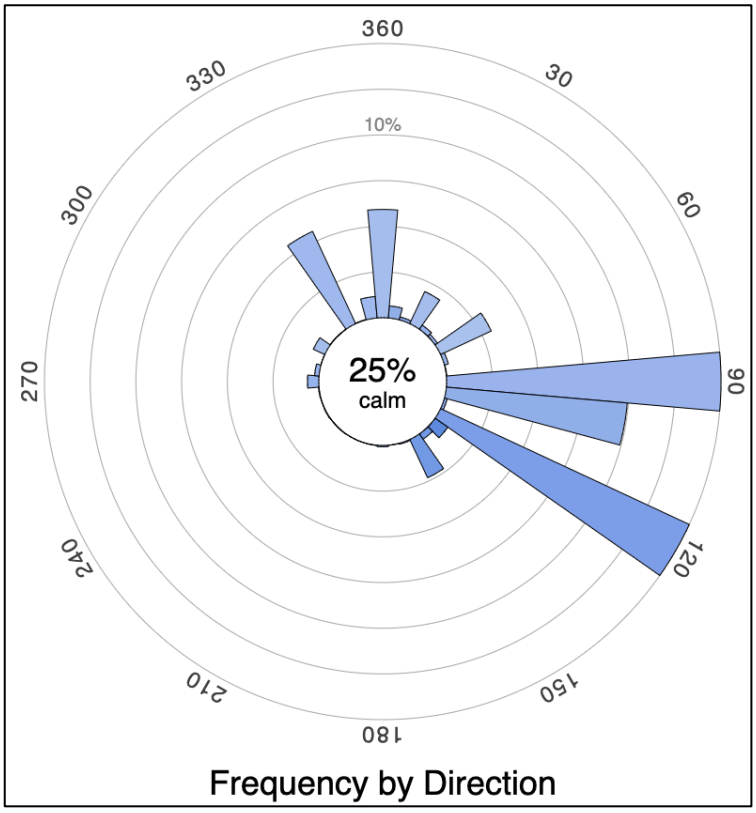

Figure 21. Wind directional frequency in Chetumal. Wind History 2011.

Total lake evapotranspiration was estimated following the MM5 weather model. The MM5 weather model is free software that allows for mesoscale climate predictions (UCAR 2003). The criteria needed for this model to accurately predict evapotranspiration include air temperature, water temperature, relative humidity, wind speed and direction, and physical size of the water body being studied. After calculating evapotranspiration values measured in m/yr, Google Earth was utilized to measure the surface area of the lake in order to estimate total evapotranspiration for 2017-2019. Evapotranspiration data and calculations are located in Appendix B.

7.8 Hydrocalculator and Meteoric Waters

The program Hydrocalculator was used as an alternative method of calculating evaporative losses from Laguna Bacalar using stable water isotopes and to quantify the LEL trend seen in Figure 16 (Skrzypek et al. 2015). Input parameters include temperature, relative humidity, precipitation, starting and final pool isotope values for $\delta^{18}O$ and $\delta^{2}H$ isotopes, and an intercept between the local evaporation line (LEL) and the global meteoric water line (GMWL) or an alternative meteoric water line. Hydrocalculator can also model both steady-state and non-steady-state bodies of water. Laguna Bacalar best fits the steady-state model because the water level is relatively stable over the course of a year and because of constant inflow to the system supplied by groundwater recharge.

Multiple MWL's have been generated in the past by other researchers including MWL's relevant specifically for Mexican meteoric waters. Problems exist with the Mexican Meteoric Water Line (MMWL) used by Wassenaar et al. (2009), for example, because many of the data

points used to generate this line come from inland and northern Mexico. This area is significantly different than the Yucatan Peninsula across a range of parameters including latitude, humidity, and elevation. Wassenaar et al. gathered inland data points and generated MMWL's heavily based on two sampling sites in the northern mainland of Mexico or averaged sites across the entire country. The isotope range found in the mainland of the country was very different than data collected on the Yucatan Peninsula and it was determined that using the MMWL produced by Wassenaar et al. was unwise when analyzing Laguna Bacalar data. Instead, the GMWL was determined to be a more fitting meteoric water line to compare against Laguna Bacalar waters. A MWL generated by Socki et al. (2002) was derived using data from sampling sites on the Yucatan Peninsula and identified as very similar to the Global Meteoric Water Line (GMWL) with a difference in slope of just 0.11. Therefore, the slope of the GMWL was selected as the optimal input for Hydrocalculator for classifying the definition of local groundwaters. Laguna Bacalar is a karst environment and groundwater is rapidly recharged from meteoric precipitation. Therefore, isotopes of the groundwater that enters the lake closely match isotopes of precipitation in this area (Socki et al. 2002).

Starting and final isotope pool values refer to two points in a body of water for which the evaporative losses will be compared. The starting isotope pool values were from Xul Ha Spring, as this is the area supplying the bulk of the water entering Laguna Bacalar. Final isotope pool were from Buena Vista, as this is the sampling site furthest to the north and water in this area was anticipated to have undergone the most evaporative loss. Based on the parameters for the sampling year entered into Hydrocalculator, the estimated evaporative loss in Xul Ha Bay is 1% whereas waters near Buena Vista have undergone approximately 15% evaporative

loss. This solidifies the hypothesis that groundwater is primarily entering the system in the southern portion of Laguna Bacalar and evaporation is the dominant hydrological process in the northern end of the lake. Hydrocalculator inputs used to calculate these evaporative losses are listed in Tables 4 and 5.

Xul Ha Pool		
Temperature (C)	26.25	
Relative Humidity (%)	76.67	
	δ^2H	$\delta^{18}O$
Pool starting values, sampling #1 (‰ VSMOW)	-24.7	-4.106
Pool final values, sampling #2 (‰ VSMOW)	-25.54	-4.4
Precipitation, mean between sampling #1 and #2 (‰ VSMOW)	-24.7	-4.106
Slope of LEL	5.48	

Buena Vista Pool		
Temperature (C)	26.17	
Relative Humidity (%)	81.9	
	δ^2H	$\delta^{18}O$
Pool starting values, sampling #1 (‰ VSMOW)	-24.7	-4.106
Pool final values, sampling #2 (‰ VSMOW)	-2.3	0.2
Precipitation, mean between sampling #1 and #2 (‰ VSMOW)	-24.7	-4.106
Slope of LEL	5.48	

Tables 4 and 5. Inputs for 2019 Hydrocalculator calculations of starting (Xul Ha) and final (Buena Vista) pools.

7.9 Major Ions and Saturation Indices

To better understand the hydrochemistry of the lake, the program PHREEQC version 3.6.2-15100 was used to analyze 2017 and 2018 hydrochemical saturation indices of the study area waters (Parkhurst and Appelo 2013). WATEQ4F was used as the thermodynamic database

and was modified to include Mg-rich calcite (Ball and Nordstrom 1991). PHREEQC utilizes field measurements to calculate aqueous species, ion activities, and mineral saturation indices to determine the tendency of a natural water to dissolve or precipitate a variety of different minerals. As seen in Tables 6 and 7, Laguna Bacalar water is oversaturated with aragonite, calcite, and dolomite, is at saturation with gypsum and amorphous silica, and is undersaturated with halite.

Saturation Indices of Select Minerals (2017 Sampling Year)						
Sampling Site	Calcite	Aragonite	Dolomite	Silicagel	Gypsum	Halite
Chaac River Outlet	0.37	0.23	0.4	-0.31	-0.22	-6.91
Chaac River	0.15	0.01	0.04	-0.31	-0.32	-6.39
Hotel Dock	0.66	0.52	1.02	-0.34	-0.29	-6.76
Cenote Bruja Bottom	-0.13	-0.27	0.2	-0.24	-0.93	-7
Cenote Bruja Middle	0.61	0.47	0.88	-0.36	-0.24	-6.91
Cenote Bruja Surface	0.47	0.33	0.61	-0.32	-0.24	-6.85
Las Palmas Main Spring	-0.14	-0.28	-0.64	-0.35	-0.32	-7.34
Las Palmas Small Spring	-0.68	-0.82	-1.69	-0.26	-0.33	-6.5

Saturation Indices of Select Minerals (2018 Sampling Year)						
Sampling Site	Calcite	Aragonite	Dolomite	Silicagel	Gypsum	Halite
Juan Carlos Well	0.04	-0.1	-0.25	-0.1	-0.21	-6.12
Xul Ha Spring	0.05	-0.09	-0.32	-0.07	-0.13	-6.79
Xul Ha Bay	0.18	0.04	-0.1	-0.08	-0.07	-6.84
Laguna Bonanza	0.15	0	-0.07	-0.08	-0.13	-6.81
Chaac River	0.51	0.37	0.68	-0.05	-0.1	-6.17
Laguna Mariscal	0.43	0.29	0.53	-0.05	-0.1	-6.2
Hotel Dock	0.38	0.24	0.44	-0.07	-0.11	-6.44
Cenote Bruja Bottom	-0.05	-0.2	-0.47	-0.08	-0.05	-6.42
Cenote Bruja Middle	-0.31	-0.45	-0.99	-0.08	-0.04	-6.42
Cenote Bruja Surface	0.03	-0.11	-0.3	-0.08	-0.05	-6.42
Lake Middle	0.53	0.39	0.71	-0.06	-0.09	-6.27
Mangrove Bay	0.37	0.23	0.45	-0.01	-0.12	-5.47
Buena Vista	0.71	0.57	1.12	-0.07	-0.13	-5.51

Tables 6 and 7. Saturation indices of select minerals for 2017 and 2018 sampling years.

This matches the observed precipitation of Mg-rich calcite. Gypsum is slightly undersaturated, but under the right conditions the lake may precipitate it in the future because of the availability of high levels of sulfate and calcium. Furthermore, Piper plots generated for these two years indicate that the local waters are rich in sulfate and calcium indicating generally calcium sulfate type waters. This agrees with Perry et al. (2002) who state that Laguna Bacalar is fed by groundwater rich in SO_4 and Ca draining from an evaporite region that contains gypsum-bearing rocks and is supersaturated with respect to calcite. The source of gypsum is from the Chicxulub impact breccia interspersed throughout the Yucatan Peninsula (Perry et al. 2002). Kenkmann and Schönian (2006) note further evidence of local gypsum in the Upper Tertiary Bacalar Formation. Waters in this area have total dissolved solid measurements ranging from 1900 to 2700 ppm of which 50-60% is sulfate. The pH range of these waters is 6.6 to 7.7. Chemical data in previously published literature for the Laguna Bacalar region is minimal, but values cited by Perry et al. (2002) are similar. Saturation indices remain relatively constant at all sampling locations with no distinct trends. Piper plots were generated using the program GW_Chart (USGS 2018) and are shown in Figures 22 and 23 (USGS 2018).

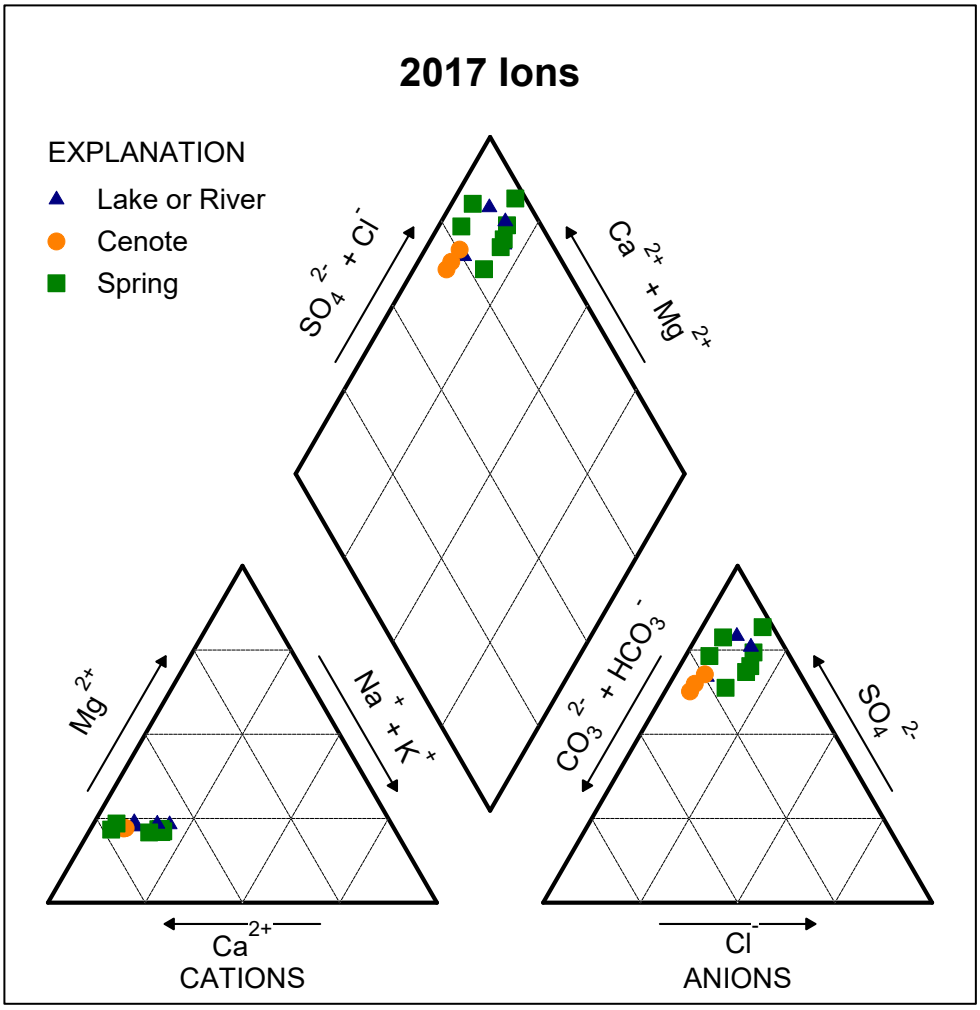

Figure 22. Piper plot of 2017 major ions. USGS 2018.

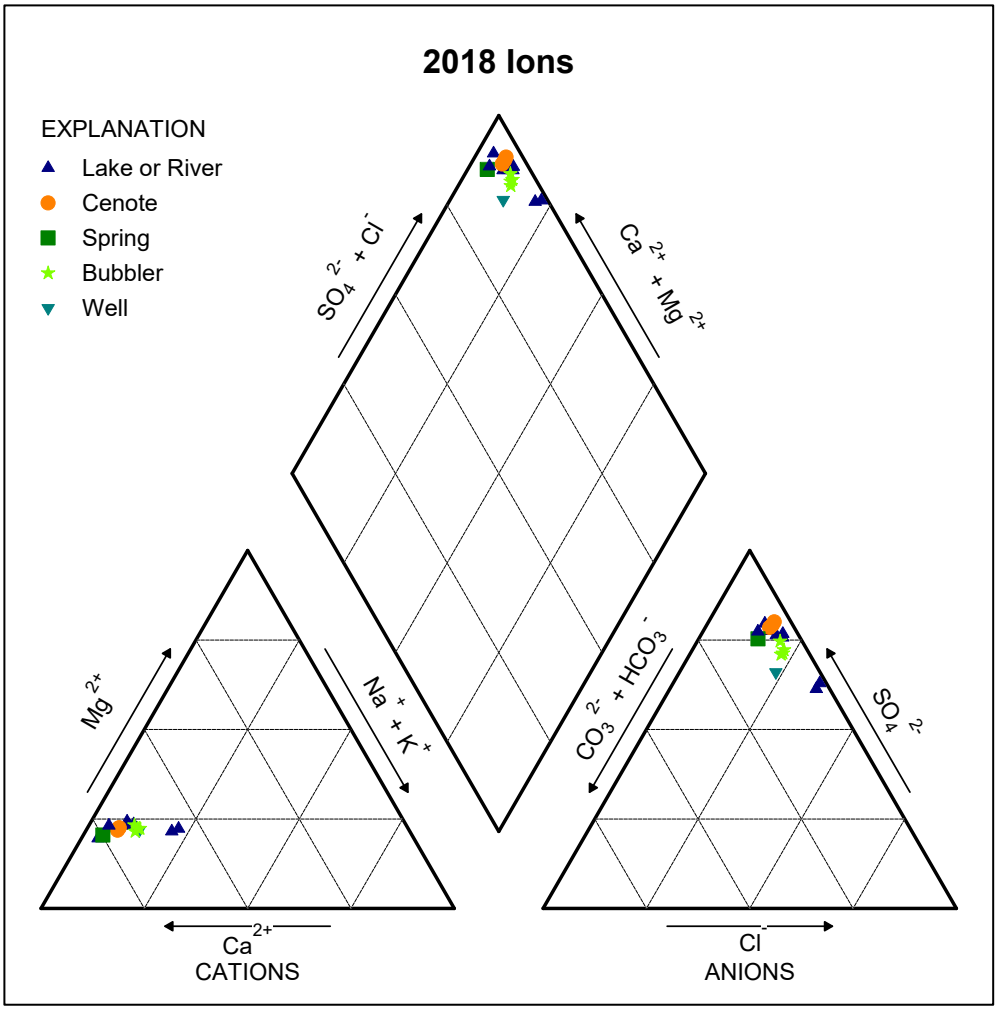

Figure 23. Piper plot of 2018 major ions. USGS 2018.

7.10 Hydrochemical Processes

Figure 24 displays 2017 and 2018 Laguna Bacalar major ion sample calculations. A standard method of analyzing the hydrochemical dominance of a carbonate-rich groundwater is through a plot of TDS versus Na/(Na+Ca). Positioning of groundwater data on this type of plot depends heavily on soil and aquifer properties. If carbonate minerals dominate the subsurface lithology, as is the case in Laguna Bacalar, groundwater chemistry will yield lower Na/(Na+Ca) values (Marandi and Shand 2018). TDS values greater than 1000 mg/L generally describe

evaporative dominance. TDS values between ~75 to 1000 mg/L depict rock weathering dominance and values below this threshold describe precipitation dominance (Zhou et al. 2017). Laguna Bacalar values indicate evaporative dominance. Literature suggests that this type of diagram can provide a general idea of hydrogeochemical activity in a groundwater but should be supplemented with Piper plots and isotope geochemistry in order to gain better insight into these processes (Marandi and Shand 2018). Both of these suggestions have been used to further understand the water chemistry of Laguna Bacalar.

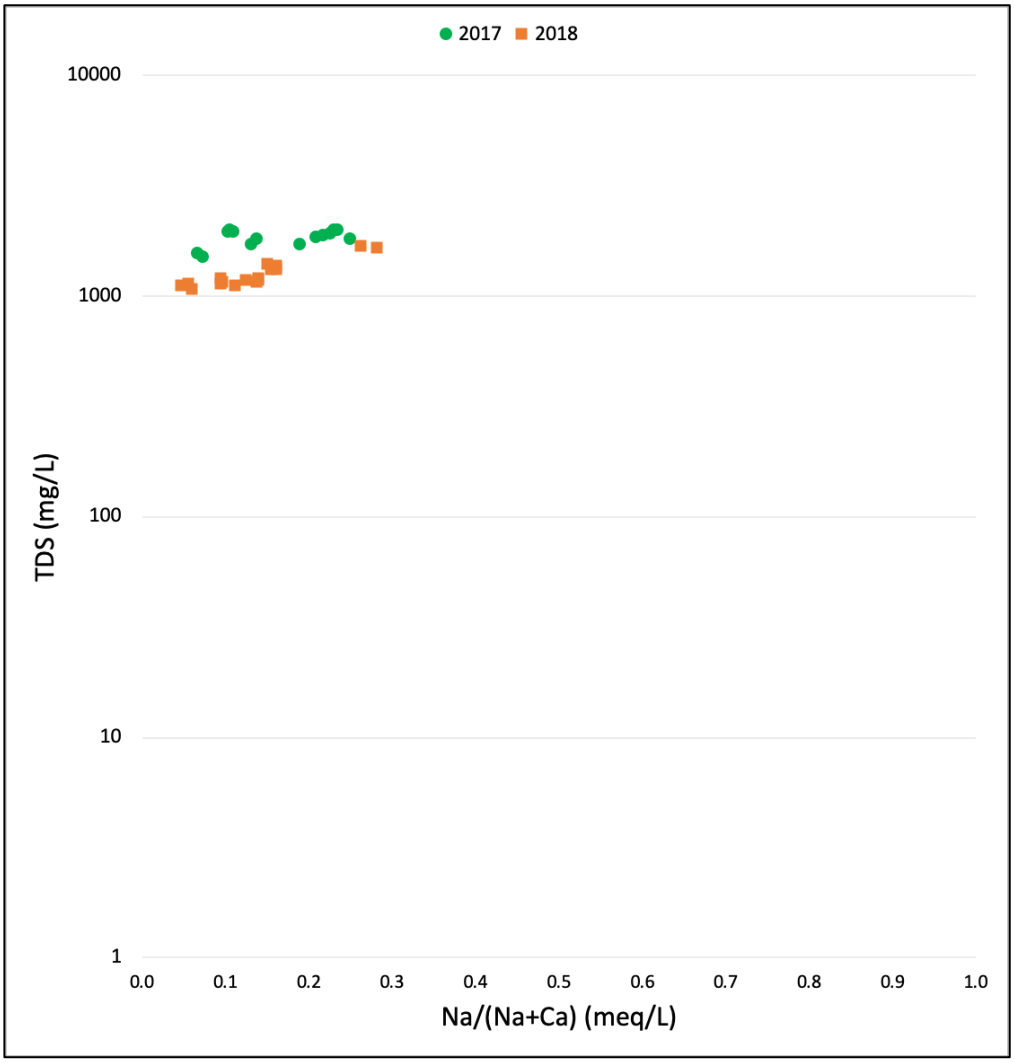

Figure 24. Plot of TDS (mg/L) vs. Na/(Na+Ca) (meq/L).

7.11 Carbon Isotopes

Carbon isotopes collected from 2017 to 2019 range from -6.48‰$_{VPDB}$ to -14.06‰$_{VPDB}$. Figure 6 of $\delta^{13}C$ in different natural compounds shows that freshwater carbonates have a $\delta^{13}C$ range from approximately -16‰$_{VPDB}$ to 4‰$_{VPDB}$. Mangroves are the most notable plant species in Laguna Bacalar and are C_3 plants. Microbially-respired CO_2 tends to mirror the $\delta^{13}C$ value of the vegetation. Generally, enriched $\delta^{13}C$ is a 50:50 mixture of dissolved carbonate bedrock and soil CO_2 dissolved during recharge. Soil CO_2 in C_3 landscapes is approximately -23‰$_{VPDB}$ (Clark and Fritz 1997). Carbon isotope samples from Xul Ha Spring averaged a $\delta^{13}C$ value of -11.3‰$_{VPDB}$. A dolomite bedrock isotope sample had a value of -0.4‰$_{VPDB}$. The median value of Laguna Bacalar carbonate bedrock sample and known C_3-type soil CO_2 is -11.7‰$_{VPDB}$. This indicates that half of the carbon in the groundwater is modern from recycled plant material and half is ancient carbon from dissolved bedrock. Carbon isotope data and calculations are located in Appendix B.

8. Discussion

Research and literature available prior to the beginning of the research outlined in this paper indicated four hypotheses regarding Laguna Bacalar hydrology.

- The bulk groundwater inflow is entering from the southern end of the lake known as Xul Ha and is supplemented by a proportion of water entering the lake from cenotes located farther north.
- The water at the north end of the lake has a negligible amount of movement and the predominant process in this area is evaporation.

- Laguna Bacalar is precipitating large amounts of calcite as is evident from hydrochemical analyses and lakebed sampling.
- Lake water has a variable residence time as evident from flow data.

Previously unstudied data sets analyzed for this paper confirmed and extrapolated upon on these hypotheses and have enabled the development of a more concrete understanding on the chemical and physical hydrology of Laguna Bacalar.

8.1 Evidence for Evaporative Processes

As evident from Figure 6, any LEL with a slope less than that of the GMWL is indicative evaporative loss from a surface water system. This is illustrated in data plotted in Figure 16 and supports the hypothesis that surface waters in the Bacalar region are undergoing significant evaporative losses. Figure 16 shows groundwater samples falling directly on the GMWL because of the recharge to this area from meteoric waters, while surface water samples that have undergone evaporation formed a LEL with a slope of 5.4, less than that of the GMWL which has a slope of 8.

Further evidence for evaporation moving northward in the lake discussed in this paper includes chloride ion concentration in water samples and significant depletion of light oxygen isotopes.

8.2 Proposed Flow

Based on the data collected from Cenote Bruja shown in Figures 18a-d and excess pCO_2 and pH trends seen in Figure 13 it is evident that the bulk inflow to Laguna Bacalar is occurring

from Xul Ha in the south plus significant input from various cenotes on the western side of the lake. Water in the northern half of the lake is stagnant and is undergoing evaporation with no water inflow from anywhere other than the southern half of the lake. A flow diagram including sources of water inflow is illustrated in Figure 25.

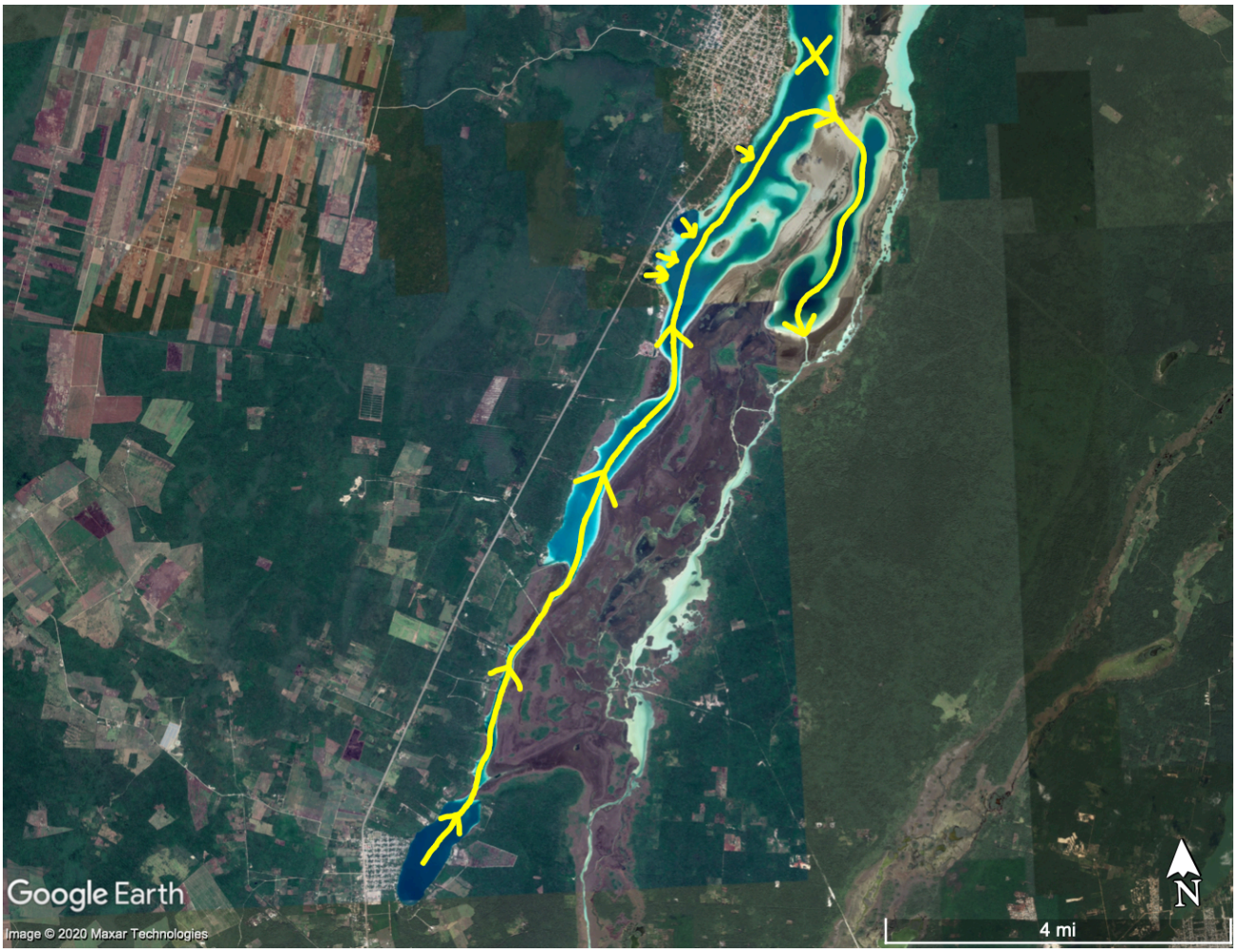

Figure 25. Schematic diagram of proposed surface water flow paths.

8.3 Residence Times

Evapotranspiration data and Hydrocalculator outputs were used in order to estimate residence times in the lake. The lake was split into three zones based on variations in hydrochemical processes and flow regime. Zones 1-3 are Xul Ha and the Rapids, the main lake body between the Rapids and Pirates' Canal, and the lake body north of Pirates' Canal, respectively. Zone 3 extends 37 km north. Figure 26 depicts the zone boundaries.

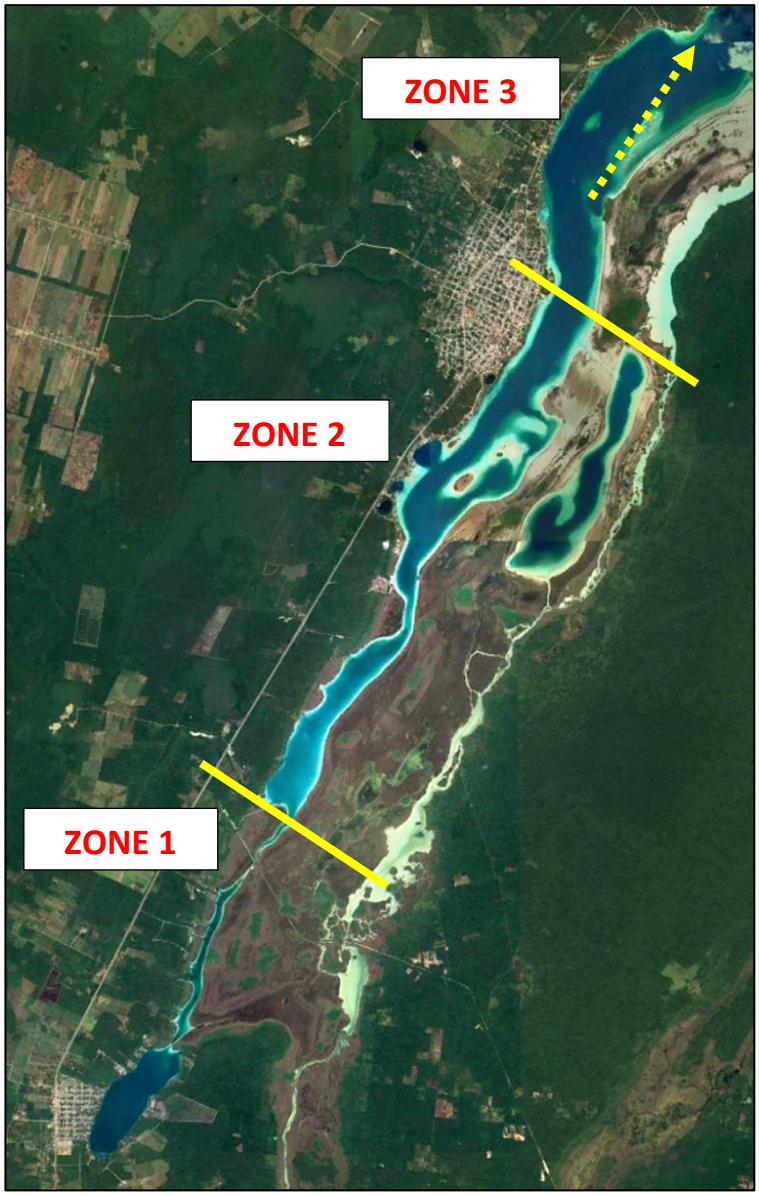

Figure 26. Zones used for residence time calculations.

A challenge that arises when attempting to estimate total water inflow and evaporative flux in the lake system is that although there are no known cenotes in the northern half of Laguna Bacalar, this system is still on top of karst bedrock. Water may be infiltrating the lake system through subsurface fractures that are presently undocumented. Section "2. Background" of this paper referenced the hypothesis put out by Perry et al. (2002) pertaining to the lack of saltwater intrusion in this area. It has been confirmed that there is massive amounts of calcite in the system through the visible observation of overabundant calcite precipitant on the lakebed, calcite precipitant yielded directly from water samples in the field through extraction for carbon isotope analysis, as well as laboratory major ion analysis and saturation indices produced using PHREEQC. The presence of this oversaturation of calcite in the lake is prohibiting chemical erosion of bedrock that would otherwise lead to lateral groundwater flow in and out of the northern half of Laguna Bacalar. If significant carbonate dissolution was occurring in this lake, saltwater intrusion would be evident from chemical analyses (Perry et al. 2002). The underlying chemical process prohibiting erosion is the common ion effect. This line of reasoning supports contention that subsurface groundwater flow entering Zone 3 is negligible when compared against the inflow from cenotes and outflow through the process of evapotranspiration due to the chemical saturation indices of the waters in the lake system that are preventing major carbonate dissolution.

Over the course of a year, the water level of Laguna Bacalar does not rise or fall significantly. Residence time calculations assume there is negligible subsurface lateral flow in and out of the lake body as noted in Section 7.7 "Evapotranspiration". Residence times for each zone were calculated using Equation 6,

$$T_r = \frac{V}{O} \quad \text{EQ. 6}$$

where T_r is residence time in yr, V is volume in m^3, and O is outflow in m^3/yr. Inflow through Zone 1 was calculated by adding the evapotranspiration and outflow through the Rapids. The residence time for this area from 2017 to 2019 is 0.30 ± 0.03 yr. Zone 2 receives inflow from the Rapids as well as the handful of cenotes on the shoreline. Cenote discharge is not known directly, but stream gauging through the Chaac River and the Rapids indicates that the higher discharge through the Chaac River is from cenotes. The cenote inflow contribution was calculated by subtracting the evapotranspiration from the Rapids inflow and then subtracting that value from the Chaac River outflow. In calculating the residence time for Zone 2 in 2019, a negative value for cenote contribution seen in Appendix B data has been deemed non-problematic because there was nearly twice the annual rainfall in this area when compared to other sampling years. Effects of this amount of rainfall on the lake was likely unnoticed by locals because it would have raised the lake level a mere 6.28 cm. The residence time in Zone 2 for 2017 to 2019 is 0.33 ± 0.03 yr. Zone 3 has no major inflow from Zone 2 and there are no known cenotes in this area, but water levels remains static throughout the year. This indicates that the inflow matches evapotranspiration. The residence time for this zone for 2017 to 2019 is 11.04 ± 0.40 yr. A table of residence time calculations is listed in Table 8 and in Appendix B.

2017	Zone 1	Zone 2	Zone 3
Surface Area (m^2)	1.95E+06	7.88E+06	4.63E+07
Depth (m)	23.8	10	10
Volume (m^3)	4.64E+07	7.88E+07	4.63E+08
ET Loss (m^3/yr) Average	1.70E+06	6.86E+06	4.03E+07
Surface Inflow (m^3/yr)	0.00E+00	1.45E+08	2.03E+07
Surface Outflow (m^3/yr)	1.45E+08	2.30E+08	0.00E+00
Precipitation Inflow (m^3/yr)	8.42E+05	3.40E+06	2.00E+07
Bulk Inflow (m^3/yr) (w.o. cenote)	1.46E+08	1.48E+08	4.03E+07
Bulk Outflow (m^3/yr)	1.47E+08	2.37E+08	4.03E+07
Other Cenote Contribution	0	8.86E+07	0
Residence Time (yr)	0.32	0.33	11.49

2018	Zone 1	Zone 2	Zone 3
Surface Area (m^2)	1.95E+06	7.88E+06	4.63E+07
Depth (m)	23.8	10	10
Volume (m^3)	4.64E+07	7.88E+07	4.63E+08
ET Loss (m^3/yr) Average	1.81E+06	7.33E+06	4.31E+07
Surface Inflow (m^3/yr)	0.00E+00	1.77E+08	1.78E+07
Surface Outflow (m^3/yr)	1.77E+08	2.49E+08	0.00E+00
Precipitation Inflow (m^3/yr)	1.07E+06	4.31E+06	2.53E+07
Bulk Inflow (m^3/yr) (w.o. cenote)	1.78E+08	1.81E+08	4.31E+07
Bulk Outflow (m^3/yr)	1.78E+08	2.56E+08	4.31E+07
Other Cenote Contribution	0	7.56E+07	0
Residence Time (yr)	0.26	0.31	10.75

2019	Zone 1	Zone 2	Zone 3
Surface Area (m^2)	1.95E+06	7.88E+06	4.63E+07
Depth (m)	23.8	10	10
Volume (m^3)	4.64E+07	7.88E+07	4.63E+08
ET Loss (m^3/yr) Average	1.79E+06	7.25E+06	4.26E+07
Surface Inflow (m^3/yr)	0.00E+00	1.45E+08	-2.91E+06
Surface Outflow (m^3/yr)	1.45E+08	2.11E+08	0.00E+00
Precipitation Inflow (m^3/yr)	1.92E+06	7.74E+06	4.55E+07
Bulk Inflow (m^3/yr) (w.o. cenote)	1.47E+08	1.53E+08	4.26E+07
Bulk Outflow (m^3/yr)	1.47E+08	2.19E+08	4.26E+07
Other Cenote Contribution	0	6.57E+07	0
Residence Time (yr)	0.32	0.36	10.87

Average Inflow (m^3/yr)	4.71E+08	4.82E+08	1.26E+08
Average ET Loss (m^3/yr) Average	5.30E+06	2.14E+07	1.26E+08
Average Residence Time (yr)	0.30	0.33	11.04
Std Dev Tr	0.03	0.03	0.40

Overall E/I	0.14

Table 8. Residence time calculations for 2017-2019 in Zones 1-3.

Although stream gauging at the nexus of cenotes and the lake body has not been performed, an estimate of cenote contribution based on specific conductivity data has been calculated using Equation 7,

$$J_C = J_R * \left[\frac{(C_{out} - C_R)}{(C_{GW} - C_{out})}\right] \quad \text{EQ. 7}$$

where J_c is inflowing groundwater from cenotes, J_R is inflow from the Rapids, C_{out} is the minimum specific conductivity measured in sonde transects in the lake, C_R is surface water conductivity in Xul Ha Embayment, and C_{GW} is the maximum specific conductivity measured in Cenote Bruja. All specific conductivity measurements are in µS/cm. Under the assumption that specific conductivities of the shoreline cenotes are relatively consistent to one another, this calculation indicates a cenote contribution to the Chaac River outflow channel of approximately 37% using 2019 data. This matches exceptionally well with the data outlined in Section 7.2 "Stream Gauging Results" and Table 1, which show a difference in flow between the Chaac River outflow and the Rapids inflow ranging from 29.1% to 37.0%.

8.4 Lake Dynamics in Summation

Through further analysis using previously unstudied data on Laguna Bacalar's physical and chemical parameters collected from 2017 to 2019, a more advanced understanding of the overall lake dynamics has emerged.

Chemical data has enabled evaporative trends to become more certain. As shown in Figure 13, CO_2 levels are above atmospheric levels throughout the entire lake. Ranging from south to north the CO_2 levels show a general trend toward atmospheric equilibrium, but some sampling locations spike up. This is explained through the addition of more CO_2 entering the system from the shoreline cenotes and possibly subsurface bedrock fractures that may allow negligible groundwater input traveling laterally from west to east, though this is not evident from chemical data. Sampling locations further from cenotes, especially in the northern end of the lake, show a steady decline in CO_2 toward atmospheric equilibrium. With the continued loss of CO_2, the trend in pH trends in the opposite direction and becomes less acidic.

Further chemical data such as chloride levels has also led to a confirmation of evaporative processes through acting as a non-evaporative chemical tracer moving north in the lake. Chloride data shows this chemical becoming more concentrated heading north as more water evaporated because chloride itself remains in the water and does not evaporate, solidifying the hypotheses on the hydrochemical processes at play and flow dynamics of the lake.

Oxygen isotope analysis further confirm the significance of evaporative processes in the lake as indicated in Figure 15. Data indicates the lake water becomes progressively depleted of lighter oxygen isotopes moving north. This is through Rayleigh-type non-equilibrium

fractionation in which lighter isotopes preferably evaporate first leaving behind water enriched with heavier isotopes.

Lake dynamics are now better understood through stream gauging and sonde profiling of Cenote Bruja. Research suggests The Chaac River is carrying more outflow than the Rapids and meteoric waters together can supply on their own. This has solidified the role of shoreline cenotes as major contributors of inflowing groundwater to the lake system and assisted in estimating lake residence times. The physical flow data along with analysis of hydrochemical data have enabled the partitioning of the lake into 3 distinct zones with varying residence times because of differences in hydrochemical processes and flow paths. Residence times have been estimated through weather modeling and evapotranspiration calculations and confirm that the northern half of the lake is largely stagnant.

9. Conclusions

Understanding the physical and chemical hydrogeology of a region is a critical step toward better decision making when applied to freshwater resources. Laguna Bacalar serves as a heavily relied upon source of water used for both drinking and recreation. Protecting these waters and the biology in this region is a goal that can only be accomplished by understanding the nature of the flow and surface water residence times of the area. Through the research laid out in this paper, a better understanding of the dynamics at play in this lake system will lead to smarter decision making regarding water management in this area and the enhancement of protection to this natural freshwater resource for both the people and wildlife relying upon it. The extremely long residence times north of the city of Bacalar point to the critical importance

of preserving water quality in the region. Although there are shorter residence times to the south where most Bacalar natives utilizing the lake spend the bulk of their time, cities like Buena Vista to the north do not have this luxury and any pollutants in the waters to the north may remain for up to 11 years.

Future work in the Laguna Bacalar region should focus on carbon isotope analysis to more accurately identify CO_2 sources and sinks. This will lead to more definitive residence times and a better understanding of calcite precipitation. More water isotope and major ion data should also be collected from both surface water and groundwater. Surface water samples should be collected from more areas of the lake in order to better identify evapotranspiration trends. Current knowledge of groundwater data beyond the shoreline cenotes is limited to one well in the region. More chemical data would help with identifying sources of gypsum dissolution that are supplying the massive amounts of sulfate to the lake. Lastly, stream gauging should continue on a monthly basis to better extrapolate knowledge on lake flow dynamics.

References

Ball, J.W., and Nordstrom, D.K. 1991. “User's Manual For WATEQ4F, With Revised Thermodynamic Data Base And Test Cases For Calculating Speciation Of Major, Trace, And Redox Elements In Natural Waters”. U.S. Geological Survey Open-File Report 91-183.

Bauer-Gottwein, P., Gondwe, B.R.N., Charvet, G., Marín, L.E., Rebolledo-Vieyra, M., and Merediz-Alonso, G. 2011. Review: The Yucatán Peninsula karst aquifer, Mexico. *Hydrogeology Journal*. 19, 507-524.

World Weather Online. 2020. “Chetumal Historical Weather”. www.worldweatheronline.com/chetumal-weather-history/quintana-roo/mx.aspx.

Clark, I., and Fritz, P. 1997. *Environmental Isotopes in Hydrogeology*.

Gondwe, B.R.N., Merediz-Alonso, G., and Bauer-Gottwein, P. 2011. *Journal of Hydrology*. 400, 24-40.

Google Earth. Laguna Bacalar, Quintana Roo, Mexico. 18.767137, -88.306882. www.earth.google.com.

Heath, R.C. 1983. Basic ground-water hydrology, U.S. Geological Survey Water-Supply Paper 2220, 13.

International Atomic Energy Agency, 2014. Groundwater Sampling Procedures for Isotope Hydrology.

Jin, L., Siegel, D.I., Lautz, L.K., Mitchell, M.J., Dahms, D.E., Mayer, B. 2010. *GSA Bulletin*. 122, 1027-1038.

SAHRA. 2005. “Oxygen”. web.sahra.arizona.edu/programs/isotopes/oxygen.html.

Kenkmann, T., and Schönian, F. 2006. Ries and Chicxulub: Impact craters on Earth provide insights for Martian ejecta blankets. *Meteoritics & Planetary Science*. 41, 1587-1603.

Kumar, S. 2018. Environmental Isotopes in Groundwater Applications. *Groundwater Development and Management*. 77-146.

Lagomasino, D., Price, R.M., Herrera-Silveira, J., Miralles-Wilhelm, F., Merediz-Alonso, G., and Gomez-Hernandez, Y. 2015. Connecting Groundwater and Surface Water Sources in Groundwater Dependent Coastal Wetlands and Estuaries: Sian Ka’an Biosphere Reserve, Quintana Roo, Mexico. *Estuaries and Coasts*. 38, 1744-1763.

Marandi, A., and Shand, P. 2018. Groundwater chemistry and the Gibbs Diagram. *Applied Geochemistry*. 97, 209-212.

Mook, W.G. 2006. *Introduction to Isotope Hydrology*. 5-18, 43-52.

Parkhurst, D.L., and Appelo, C.A.J., 2013. Description of input and examples for PHREEQC version 3–A computer program for speciation, batch-reaction, one-dimensional transport, and inverse geochemical calculations. Volume book 6 series Techniques and Methods.

Perry, E., Paytan, A., Pedersen, B., and Velazquez-Oliman, G. 2009. Groundwater geochemistry of the Yucatan Peninsula, Mexico: Constraints on stratigraphy and hydrogeology. *Journal of Hydrology*. 367, 27-40.

Perry, E., Velazquez-Oliman, G., and Marin, L. 2002. The Hydrogeochemistry of the Karst Aquifer System of the Northern Yucatan Peninsula, Mexico. *International Geology Review*. 44(3), 191-221.

Rozencrantz, E. 1990. Structure and Tectonics of the Yucatan Basin, Caribbean Sea, as Determined from Seismic Reflection Studies. *Tectonics*. 9(5), 1037-1059.

Sánchez, J.A., Álvarez, T., Pacheco, J.G., Carrillo, L., and González, R.A. 2016. Groundwater Quality: Quintana Roo, Mexico, Southern Aquifer. *Water Technology and Sciences*. 7(4), 75-96.

Schönian, F., Tagle, R., Stöffler, D., Kenkmann, T. 2005. Geology of Southern Quintana Roo (Mexico) and the Chicxulub Ejecta Blanket. *Lunar and Planetary Science XXXVI*. Conference Paper.

Skrzypek, G., Mydłowski, A., Dogramaci, S., Hedley, P., Gibson, J.J., Grierson, P.F., 2015. Estimation of evaporative loss based on the stable isotope composition of water using Hydrocalculator. *Journal of Hydrology* 523, 781–789.

Socki, R.A., Perry, E.C., Romanek, C.S., 2002. Stable isotope systematics of two cenotes from the northern Yucatan Peninsula, Mexico. *Limnol. Oceanogr.* 47(6), 1808-1818.

UCAR. 2003. “MM5 Community Model Homepage”. a.atmos.washington.edu/~ovens/newwebpage/mm5-home.html.

US EPA. 1993. Method 300.0 Determination of Inorganic Anions by Ion Chromatography.

US EPA. 1986. Method 7140 Calcium (Atomic Absorption, Direct Aspiration).

US EPA. 1986. Method 7450 Magnesium (Atomic Absorption, Direct Aspiration).

US EPA. 1986. Method 7610 Potassium (Atomic Absorption, Direct Aspiration).

US EPA. 1986. Method 7770 Sodium (Atomic Absorption, Direct Aspiration).

USGS. 2013. “Methods for Alkalinity Calculator”. https://or.water.usgs.gov/alk/methods.html.

USGS. 2018. “GW_Chart: A Program for Creating Specialized Graphs Used in Groundwater Studies”. www.usgs.gov/software/gwchart-a-program-creating-specialized-graphs-used-groundwater-studies.

Wassenaar, L.I., Van Wilgenburg, S.L., Larson, K., Hobson, K.A. 2009. A groundwater isoscape (δD, δ18O) for Mexico. *Journal of Geochemical Exploration*. 102, 123-136.

Wind History. 2011. “MMCM: Chetumal, Q. ROO”. windhistory.com/station.html?MMCM.

World Meteorological Organization. 2010. Manual on Stream Gauging, 1, 5.1-5.3. No. 1044.

Zhou, P., Li, M., and Lu, Y., 2017. Hydrochemistry and Isotope Hydrology for Groundwater Sustainability of the Coastal Multilayered Aquifer System (Zhanjiang, China). *Geofluids*. 2017, Article ID 7080346.

Appendices

Appendix A – Methods and Sampling Locations

Anion Methods

US EPA. 1986. Method 7140 Calcium (Atomic Absorption, Direct Aspiration).

US EPA. 1986. Method 7450 Magnesium (Atomic Absorption, Direct Aspiration).

US EPA. 1986. Method 7610 Potassium (Atomic Absorption, Direct Aspiration).

US EPA. 1986. Method 7770 Sodium (Atomic Absorption, Direct Aspiration).

Cations Methods

US EPA. 1993. Method 300.0 Determination of Inorganic Anions by Ion Chromatography.

Stream Gauge Methods

World Meteorological Organization. 2010. Manual on Stream Gauging, 1, 5.1-5.3. No. 1044.

Water and Carbon Isotope Sampling

International Atomic Energy Agency, 2014. Groundwater Sampling Procedures for Isotope Hydrology.

Appendix A – Data Locations

Ca:Mg Ratio Sediment Sample Locations

Sample Name	Latitude	Longitude	Location Description
SED A	18.7678	-88.299	Paradise Bay (Lake Sediment)
JJ1	18.64766	-88.39658	Middle Lake East Side (Stromatolite Core)
JJ2	18.61383	-88.42595	South Lake West Side (Stromatolite Core)
JJ3	18.58834	-88.43537	The Rapids (Stromatolite Core)

2017 Major Ion Sampling Locations

Sample Name	Latitude	Longitude
Hotelito Amigos Dock	18.6729	-88.3842
Negro Cenote Bottom	18.66722	-88.39527
Chaac River Outlet 2016	18.625	-88.391
Spring by Jim's house	18.6891	-88.3846
Negro Cenote Middle	18.66722	-88.39527
Negro Cenote Top Sample	18.66722	-88.39527
Chaac River	18.625	-88.391
Las Palmas Small Spring	18.686	-88.384
Las Palmas Main Spring	18.686	-88.384
Rich Core	18.657222	-88.391389
Chaac River	18.623583	-88.391405
Rapids	18.58959	-88.434472
Cenote Esmerelda	18.655047	-88.40557
Cenote Cocolitos	18.649862	-88.410344

2018 Major Ion Sampling Locations

Sampling Site Name	Latitude	Longitude
Juan Carlos Well	18.7701	-88.3925
Laguna Bonanza	18.5861	-88.4401
Xul Ha Embayment	18.5489	-88.4611
Xul Ha Spring	18.5469	-88.4558
Cenote Bruja surface	18.6671	-88.3944
Cenote Bruja 15m off bottom	18.6671	-88.3944
Cenote Bruja Bottom	18.6671	-88.3944
Hotelito Amigos Dock	18.6729	-88.3842
Groundwater Bubbler #1	18.6891	-88.3846
Groundwater Bubbler #2	18.6891	-88.3846
Groundwater Bubbler #3	18.6891	-88.3846
Groundwater Bubbler Surface	18.6891	-88.3846
Laguna Bacalar Middle	18.673	-88.384
Laguna Mariscal	18.6631	-88.3729
Chaac River	18.6231	-88.3908
Buena Vista	18.8788	-88.2372
Mangrove Bay (Paradise)	18.7678	-88.299

2017 Carbon Isotope Sampling Locations

Sampling Site Name	Latitude	Longitude
Chaac River Gauge Station	18.625	-88.391
Xul Ha Spring	18.543	-88.461
Mid Lake (Bacalar)	18.673	-88.384
Oncoid Sample (500m SE of Gauge Station)	18.622	-88.391
Juan Carlos Well Cuttings	18.770	-88.392
Hotel Amigos Dock	18.664	-88.395
Buena Vista	18.879	-88.237
Xul Ha Embayment	18.550	-88.456
Mangrove Bay Oncoid	18.766	-88.298
Mangrove Bay Sediment (Paradise)	18.768	-88.299

2018 Carbon Isotope Sampling Locations

Sampling Site Name	Latitude	Longitude
Xul Ha Spring	18.543	-88.461
Mid-Lake	18.673	-88.384
Oncoid Sample	18.622	-88.391
Juan Carlos Well Cuttings	18.770	-88.392
Hotel Amigos Dock	18.664	-88.395
Buena Vista	18.879	-88.237
Xul Ha Embayment	18.55	-88.456
Mangrove Oncoid	18.766	-88.298
Mangrove Bay Sediment (Paradise)	18.768	-88.299

2019 Carbon Isotope Sampling Locations

Sampling Site Name	Latitude	Longitude
CB19 10M	18.6678	-88.3947
CB19 30M	18.6678	-88.3947
CB19 50M	18.6678	-88.3947
ML19	18.6517	-88.4018
LM19	18.6408	-88.3816
BV19	18.87879	-88.23703

2017 Water Isotope Sampling Locations

Sample Location	Latitude	Longitude
Xul Ha Spring	18.543	-88.461
Negro Cenote Top	18.667	-88.394
Negro Cenote Middle	18.667	-88.394
Negro Cenote Bottom	18.667	-88.394
Balneario Park	18.681	-88.383
Laguna Mariscal Proper	18.664	-88.372
Laguna Mariscal Middle	18.652	-88.377
Laguna Mariscal South	18.659	-88.384
Bottom of Laguna Mariscal	18.659	-88.384
Chaac River	18.625	-88.391

2018 Water Isotope Sampling Locations

Sampling Site Name	Latitude	Longitude
Juan Carlos Well	18.77017	-88.3925
Laguna Bonanza	18.5861	-88.4401
Xul Ha Embayment	18.5489	-88.4611
Xul Ha Spring	18.5469	-88.4558
Cenote Bruja surface	18.6671	-88.3944
Cenote Bruja 15m off bottom	18.6671	-88.3944
Cenote Bruja Bottom	18.6671	-88.3944
Hotelito Amigos Dock	18.6729	-88.3842
Groundwater Bubbler #1	18.6891	-88.3846
Groundwater Bubbler #2	18.6891	-88.3846
Groundwater Bubbler #3	18.6891	-88.3846
Groundwater Bubbler Surface	18.6891	-88.3846
Laguna Bacalar Middle	18.673	-88.384
Laguna Mariscal	18.6631	-88.3729
Chaac River	18.6231	-88.3908
Buena Vista	18.8788	-88.2372
Mangrove Bay (Paradise)	18.7678	-88.299

2019 Water Isotope Sampling Locations

Sampling Site Name	Latitude	Longitude
CB19 Surface	18.6678	-88.3947
CB19 10M	18.6678	-88.3947
CB19 30M	18.6678	-88.3947
CB19 50M	18.6678	-88.3947
CA19	18.6471	-88.4126
ML19	18.6517	-88.4018
LM19	18.6408	-88.3816
BV19	18.8787	-88.2370
XH19	18.5491	-88.4573

Stream Gauge Locations

Sampling Site Name	Latitude	Longitude
Chaac River	18.625	-88.391
The Rapids	18.5883	-88.4355

Appendix B – Field and Analytical Results

Appendix A – Field and Analytical Results

2017 Major Ion Data

Sample Name	Ca (mg/L)	Mg (mg/L)	Na (mg/L)	K (mg/L)	HCO3 (mg/L)	Cl (mg/L)	SO4 (mg/L)	NO3 (mg/L)	Silica (mg/L)	TDS	pH
Hotelito Amigos Dock	422.33	87.19	78.31	3.43	519.72	106.74	1123.35	1.73	29.70	2342.80	6.98
Negro Cenote Bottom	457.70	88.61	63.24	3.28	702.72	93.47	1260.68	2.01	36.26	2671.71	6.73
Chaac River Outlet 2016	352.25	86.84	136.17	4.90	231.80	194.01	1032.13	1.06	31.86	1807.36	7
Spring by Jim's house	428.50	90.20	148.42	6.70	230.58	208.80	1094.56	3.47	32.42	2211.23	6.9
Panatona #4 Surface	387.49	84.90	67.72	2.99	178.73	100.56	1050.24	1.62	28.36	1874.25	7
Negro Cenote Middle	473.22	90.72	64.29	3.16	773.48	93.55	1237.47	1.84	27.86	2737.73	6.73
Negro Cenote Top Sample	461.95	90.00	66.86	3.18	560.59	102.64	1219.83	11.95	30.48	2517.00	6.73
Spring by Jim's house	399.44	88.35	135.21	5.02	453.84	187.96	1076.31	3.95	30.90	2350.08	7
Spring by Jim's house	419.14	90.19	149.29	7.68	278.16	213.36	1102.18	5.64	31.18	2265.64	6.89
Spring by Jim's house	402.73	87.69	129.13	6.73	159.82	180.43	1069.12	6.92	33.40	2042.57	7.11
Palmar Spring	379.00	76.50	35.22	1.87	336.11	58.38	940.25	3.57	38.68	1494.79	7
L. Guerrero Manatee Preserve	421.28	161.02	818.20	17.81	550.83	1256.42	1235.81	9.14	30.92	3919.68	7.5
Chaac River	381.21	89.71	116.63	5.07	158.60	165.33	1100.21	1.16	31.70	2017.92	7
Las Palmas Small Spring	400.85	79.69	108.41	7.95	39.65	134.75	958.46	4.13	35.84	1733.89	6.72
Las Palmas Main Spring	414.95	74.79	34.62	1.76	221.43	61.81	954.46	3.35	29	1767.17	6.51
Chetumal Bay	1168.78	346.58	1853.26	78.27	2886.40	3254.40	1460.88	0.00	27.06	8162.17	8.33

2018 Major Ion Data

Sample Name	Ca (mg/L)	Mg (mg/L)	Na (mg/L)	K (mg/L)	HCO3 (mg/L)	Cl (mg/L)	SO4 (mg/L)	Silica (mg/L)	pH
Juan Carlos Well	457.4	92.9	102.8	0.8	280.6	355.3	1364.9	48.11	6.64
Laguna Bonanza	493.8	96.4	38.2	0.3	237.9	196.2	1549.1	49.69	6.81
Xul Ha Spring	545.5	90.6	39.5	0.3	244.0	197.1	1400.5	53.25	6.62
Xul Ha Embayment	607.7	94.4	36.2	0.3	158.6	193.1	1507.4	49.55	6.92
Cenote Bruja Surface	555.0	107.6	68.7	0.5	176.9	270.7	1848.1	50.15	6.8
Cenote Bruja 15m	564.6	106.1	69.6	0.4	115.9	267.5	1823.9	49.73	6.64
Cenote Bruja Bottom	550.9	108.1	69.6	0.5	140.3	268.5	1809.2	49.51	6.82
Hotelito Amigos Dock	477.6	104.9	70.9	0.5	189.1	264.6	1748.5	48.77	7.2
GW Bubbler #1	522.6	109.1	117.1	0.6	213.5	398.0	1729.1	52.61	6.88
GW Bubbler #2	525.8	108.7	112.5	0.6	170.8	393.0	1732.1	52.17	7.07
GW Bubbler #3	562.2	110.5	116.5	0.6	195.2	401.9	1733.5	53.93	7.07
Bubbler Surface	492.6	105.8	93.7	0.5	152.5	336.1	1694.9	50.61	7.5
Lake Middle	496.3	103.8	83.4	0.5	158.6	311.6	1767.0	49.87	7.42
Laguna Mariscal	498.4	108.1	92.7	0.5	103.7	327.8	1732.7	49.95	7.51
Chaac River	502.3	106.6	96.2	0.5	122.0	337.1	1719.9	50.31	7.51
Buena Vista	525.6	119.0	217.7	1.0	109.8	703.0	1646.5	51.63	7.72
Mangrove Bay	499.2	121.2	227.7	1.0	54.9	728.3	1747.8	54.43	7.75

Sediment XRD Images

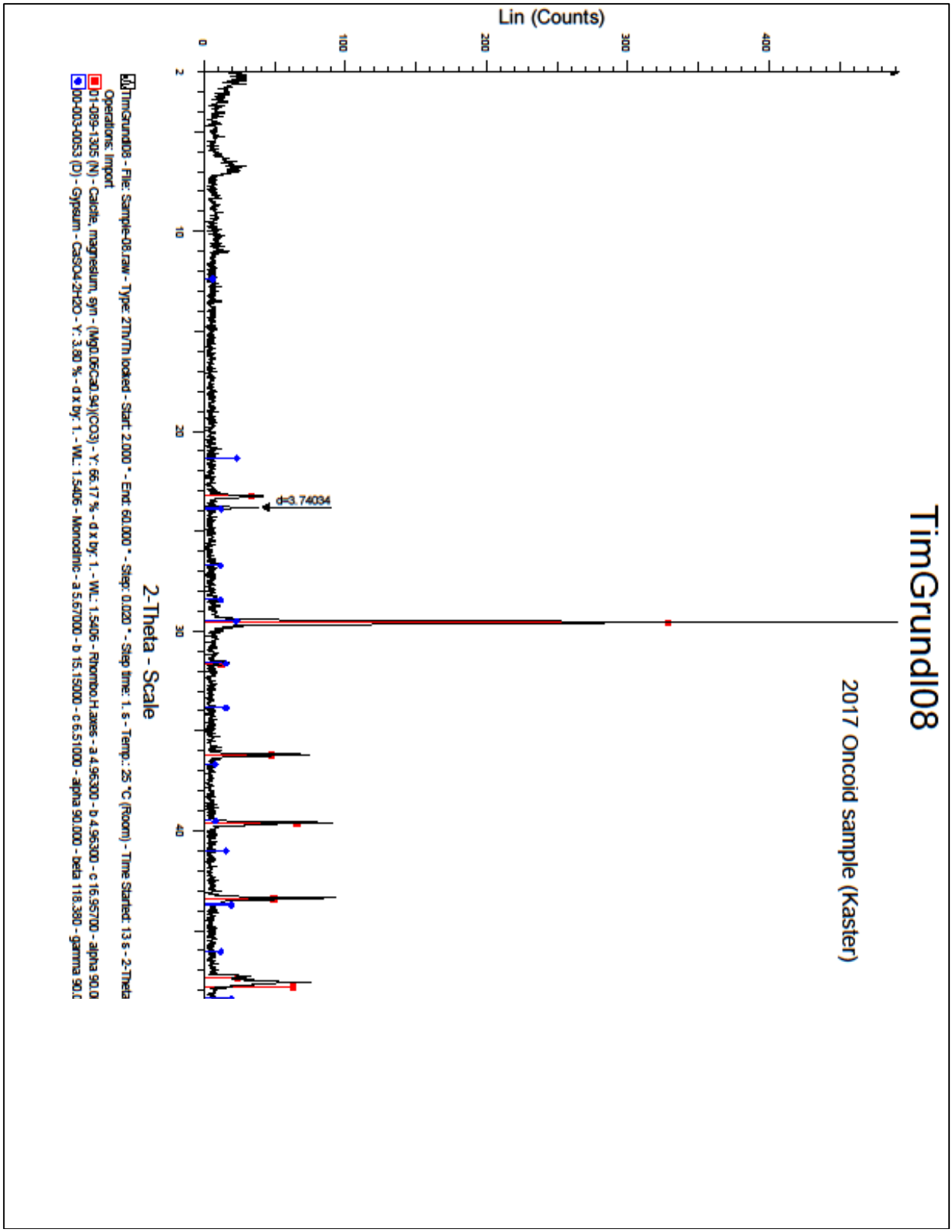

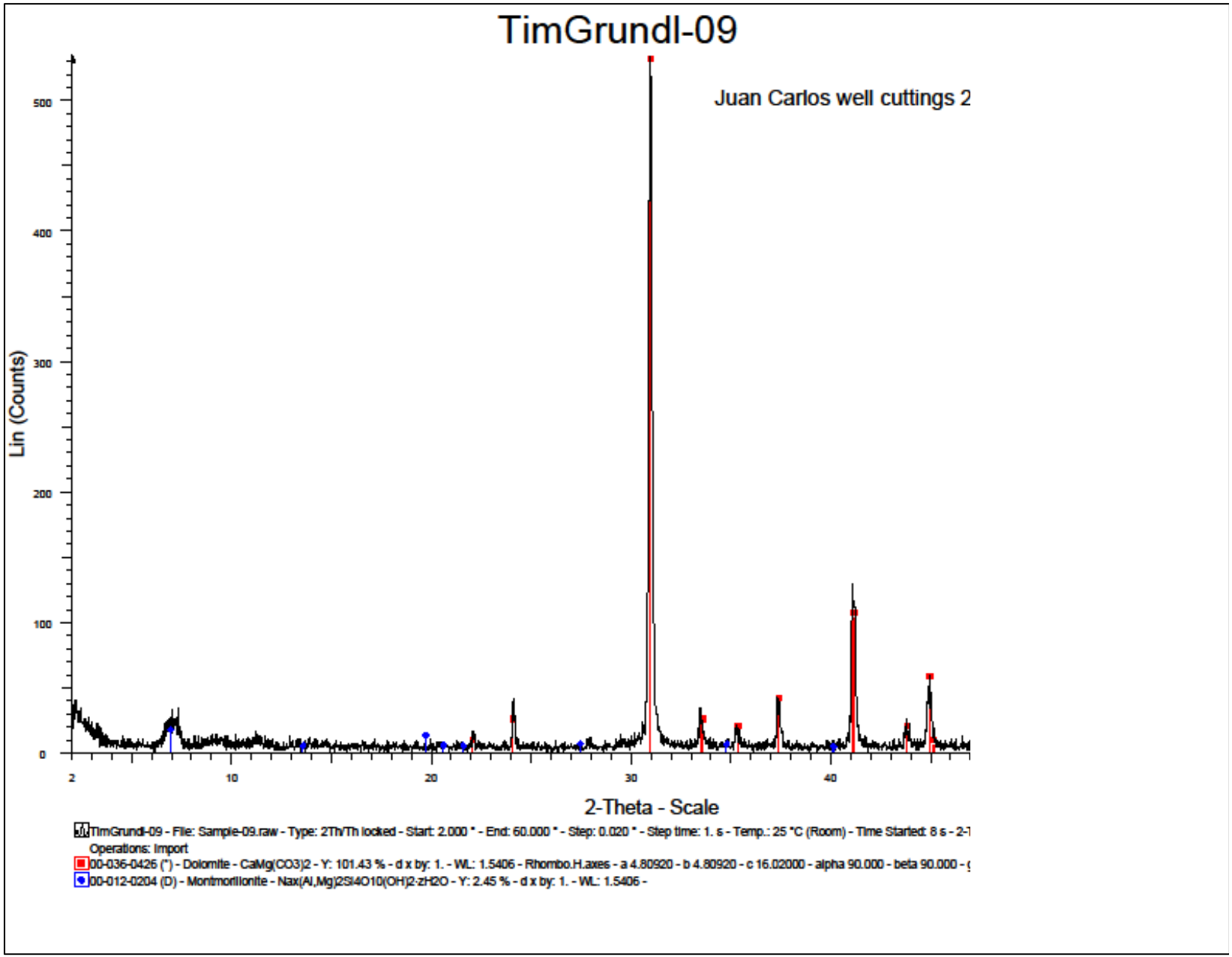
TimGrundl-09
Juan Carlos well cuttings 2
Lin (Counts)
0
100
200
300
400
500
2
10
20
30
40
2-Theta - Scale
TimGrundl-09 - File: Sample-09.raw - Type: 2Th/Th locked - Start: 2.000 ° - End: 60.000 ° - Step: 0.020 ° - Step time: 1. s - Temp.: 25 °C (Room) - Time Started: 8 s - 2-T
Operations: Import
00-036-0426 (*) - Dolomite - CaMg(CO3)2 - Y: 101.43 % - d x by: 1. - WL: 1.5406 - Rhombo.H.axes - a 4.80920 - b 4.80920 - c 16.02000 - alpha 90.000 - beta 90.000 -
00-012-0204 (D) - Montmorillonite - Nax(Al,Mg)2Si4O10(OH)2·zH2O - Y: 2.45 % - d x by: 1. - WL: 1.5406 -

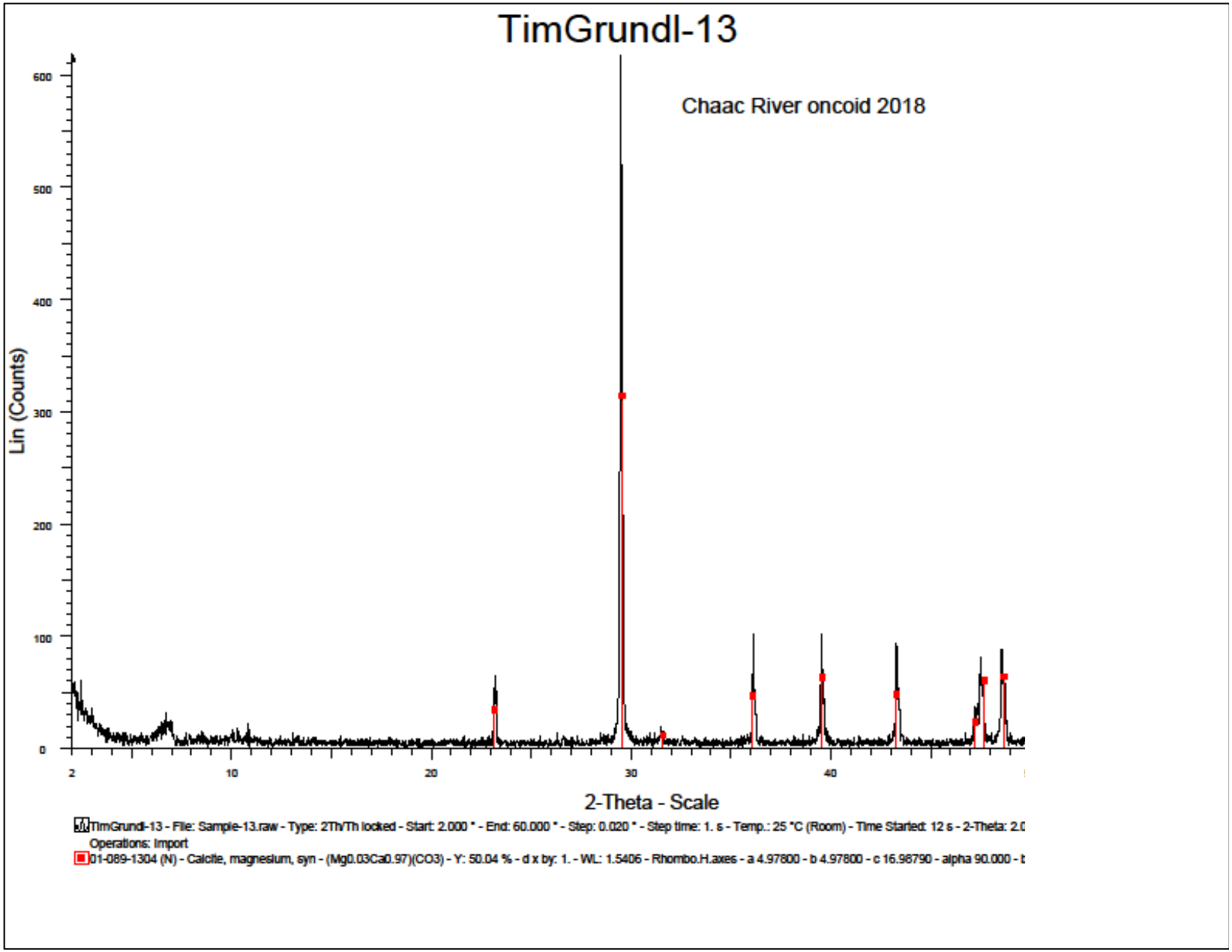
TimGrundl-13
Chaac River oncoid 2018
Lin (Counts)
600
500
400
300
200
100
0
2
10
20
30
40
2-Theta - Scale
TimGrundl-13 - File: Sample-13.raw - Type: 2Th/Th locked - Start: 2.000 ° - End: 60.000 ° - Step: 0.020 ° - Step time: 1. s - Temp.: 25 °C (Room) - Time Started: 12 s - 2-Theta: 2.0
Operations: Import
01-089-1304 (N) - Calcite, magnesium, syn - (Mg0.03Ca0.97)(CO3) - Y: 50.04 % - d x by: 1. - WL: 1.5406 - Rhombo.H.axes - a 4.97800 - b 4.97800 - c 16.96790 - alpha 90.000 - b

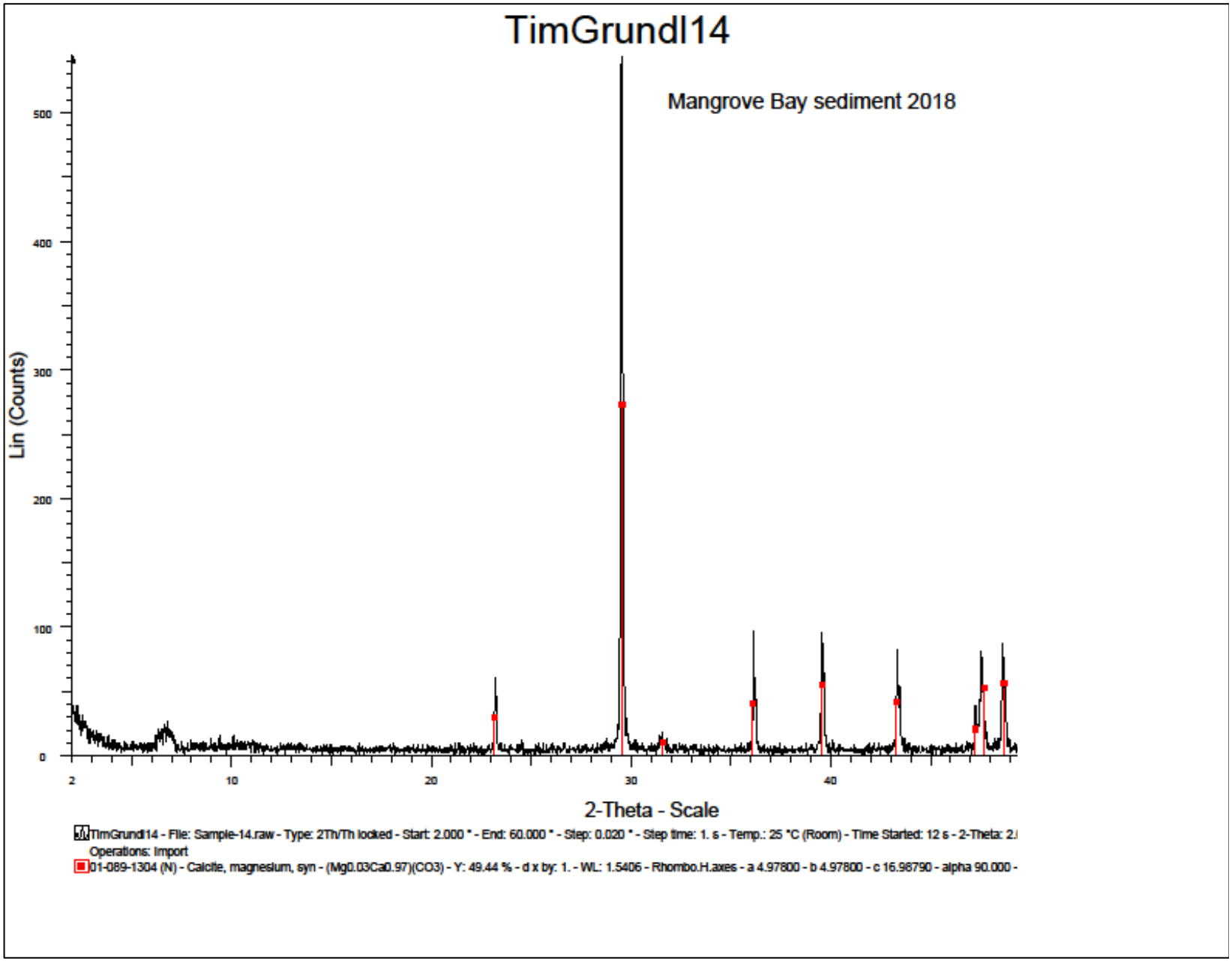
TimGrundl14
Mangrove Bay sediment 2018
Lin (Counts)
0
100
200
300
400
500
2
10
20
30
40
2-Theta - Scale
TimGrundl14 - File: Sample-14.raw - Type: 2Th/Th locked - Start: 2.000 ° - End: 60.000 ° - Step: 0.020 ° - Step time: 1. s - Temp.: 25 °C (Room) - Time Started: 12 s - 2-Theta: 2.
Operations: Import
01-089-1304 (N) - Calcite, magnesium, syn - (Mg0.03Ca0.97)(CO3) - Y: 49.44 % - d x by: 1. - WL: 1.5406 - Rhombo.H.axes - a 4.97800 - b 4.97800 - c 16.98790 - alpha 90.000 -

Ca:Mg Sediment Ratio Data

Sample Names	Ca (Dilution 1:100) Corrected Conc (mg/L)	Mg (Dilution 1:100) Corrected Conc (mg/L)	Ca:Mg Ratio
SED A	959.083	32.499	29.5
JJ1	897.797	27.285	32.9
JJ2	938.153	35.430	26.5
JJ3	929.376	25.208	36.9

Laguna Bacalar Lake Temperatures Feb-Nov 2015 (Buena Vista Site)

Month	Temp (Deg C)
Feb	25.84
Mar	27.80
Apr	29.04
May	29.81
Jun	29.59
Jul	30.36
Aug	31.30
Sep	30.97
Oct	30.15
Nov	29.48
Average	27.07

Laguna Bacalar Lake Temperatures Feb-Nov 2015 (Marzo Poli Site)

Month	Temp (Deg C)
Feb	26.44
Mar	28.08
Apr	29.10
May	29.37
Jun	29.41
Jul	30.16
Aug	30.98
Sep	30.49
Oct	29.79
Nov	29.16

Water Isotope Data – 2017

Sample Location	δ18O ‰	δD ‰
Xul Ha Spring	-4.17	-24.34
Negro Cenote Top	-4.21	-24.89
Negro Cenote Middle	-4.17	-24.12
Negro Cenote Bottom	-4.11	-23.64
Balneario Park	-2.30	-14.18
Laguna Mariscal Proper	-2.26	-14.11
Laguna Mariscal Middle	-1.77	-12.31
Laguna Mariscal south	-0.78	-7.09
Bottom of Laguna Mariscal	-2.85	-17.57
Chaac River	-1.04	-6.71

Water Isotope Data – 2018

Sample Name	Sample Description	δ18O ‰	δD ‰
5-JCW-18	Juan Carlos Well	-5.08	-30.73
17-LB-18	Laguna Bonanza (near the Rapids)	-4.44	-26.45
12-XH-18	Xul Ha Embayment	-4.40	-25.54
16-XHS-18	Xul Ha Spring	-4.26	-25.99
15-CBS-18	Cenote Bruja Surface	-4.00	-23.24
13-CB15-18	Cenote Bruja 15M Off Bottom	-3.91	-23.04
14-CBB-18	Cenote Bruja Bottom	-3.87	-22.86
1-HAD-18	Hotelito Amigos Dock	-3.61	-23.10
9-GB1-18	Groundwater Bubbler #1	-3.18	-19.38
7-GB3-18	Groundwater Bubbler #2	-3.15	-18.54
10-GB2-18	Groundwater Bubbler #3	-3.17	-20.22
8-SAB-18	Groundwater Bubbler Surface	-2.66	-16.63
2-LBM-18	Laguna Bacalar Middle	-2.58	-17.57
4-LM-18	Laguna Mariscal	-2.26	-14.62
3-CR-18	Chaac River	-1.98	-12.73
6-BV-18	Buena Vista	-0.42	-4.44
11-MB-18	Mangrove Bay (Paradise)	0.36	0.98

Water Isotope Data - 2019

Sample Name	Sample Description	δ18O ‰	δD ‰
CB19 SURFACE	Cenote Bruja Surface	-2.6	-20.9
CB19 10 M	Cenote Bruja 10M	-0.5	-18.2
CB19 50M	Cenote Bruja 30M	-1.5	-18.0
XH19	Xul Ha Embayment	-1.2	-17.7
BV19	Buena Vista	0.2	-2.3
LM19	Laguna Mariscal	0.0	-6.9
ML19	Mid Lake	-1.5	-15.0
CA19	Cenote Azul	-2.9	-23.0

Evapotranspiration Calculations and Climate Data

Air Temp (Deg C)				Water Temp (C)	Difference (C)
Month	2017	2018	2019	Average	Water-Air
Jan	25.2	22.6	23.3	27.2	3.5
Feb	26.7	25.9	26.3	26.1	-0.2
Mar	26.6	26.2	26.5	27.9	1.5
Apr	28.1	27.4	27.8	29.1	1.3
May	29.0	28.2	29.2	29.6	0.8
Jun	28.5	28.4	29.2	29.5	0.8
Jul	28.7	28.8	29.6	30.3	1.2
Aug	29.1	28.5	29.9	31.1	1.9
Sep	29.2	28.2	29.2	30.7	1.9
Oct	26.3	27.4	28.1	30.0	2.7
Nov	24.6	26.2	26.4	29.3	3.6
Dec	24.1	24.7	25.2	28.3	3.7
Average	27.2	26.9	27.6	29.1	1.9
Std Dev	1.77	1.86	2.05	1.47	1.25

T-Ts (Air Temp-Water Temp, Deg C)			
Month	2017	2018	2019
Jan	-2.0	-4.6	-3.9
Feb	0.6	-0.2	0.2
Mar	-1.3	-1.7	-1.5
Apr	-1.0	-1.6	-1.3
May	-0.6	-1.4	-0.4
Jun	-1.0	-1.1	-0.3
Jul	-1.5	-1.5	-0.6
Aug	-2.0	-2.6	-1.2
Sep	-1.6	-2.5	-1.5
Oct	-3.6	-2.6	-1.9
Nov	-4.7	-3.1	-2.9
Dec	-4.2	-3.6	-3.1
Average	-1.9	-2.2	-1.5
Std Dev	0.87	0.93	0.92

Wind Speed (m/s)				Primary Wind Direction
Month	2017	2018	2019	(deg, % frequency)
Jan	3.37	2.00	1.90	90, 27%
Feb	3.92	3.21	4.33	90/120, 23%
Mar	3.97	4.34	3.90	90/120, 16%
Apr	4.98	4.51	4.69	90/100/120, 13%
May	4.96	3.33	5.40	90/120, 16%
Jun	3.99	4.80	5.03	90/120, 20%
Jul	2.85	3.54	4.26	90/100/120, 21%
Aug	3.58	3.50	4.51	90/120, 26%
Sep	2.77	2.40	2.71	90/120, 30%
Oct	1.64	2.11	2.66	330/90/120, 35%
Nov	1.37	2.74	1.66	330/360, 39%
Dec	1.53	2.74	2.19	330/90, 36%
Average	3.24	3.27	3.61	Average Distance of Wind over Water
Std Dev	1.19	0.93	1.30	.953 km

Relative Humidity			
Month	2017	2018	2019
Jan	75	79	80
Feb	74	80	79
Mar	71	74	71
Apr	73	75	74
May	73	74	75
Jun	77	79	76
Jul	75	78	75
Aug	80	80	76
Sep	80	81	79
Oct	82	86	82
Nov	80	84	82
Dec	80	81	79
Average	76.67	79.25	77.33
Std Dev	3.63	3.70	3.37

Air Temp Daily (C)	2017		2018		2019	
Month	Average	StDev	Average	StDev	Average	StDev
Jan	25.16	1.87	22.57	1.77	23.27	2.01
Feb	26.74	0.92	25.92	1.03	26.35	1.11
Mar	26.62	0.98	26.22	1.18	26.49	1.15
Apr	28.12	1.12	27.44	1.35	27.77	1.15
May	29.00	1.06	28.24	0.97	29.22	0.51
Jun	28.51	1.24	28.38	1.08	29.19	1.14
Jul	28.75	1.01	28.77	1.17	29.64	0.98
Aug	29.13	1.41	28.55	1.06	29.91	0.81
Sep	29.15	0.90	28.25	1.05	29.24	0.95
Oct	26.33	1.79	27.36	1.09	28.06	1.32
Nov	24.65	1.35	26.21	1.84	26.38	1.82
Dec	24.08	2.23	24.69	2.22	25.17	2.15
AVERAGE	27.19		26.88		27.56	

Precipitation (mm)			
Month	2017	2018	2019
Jan	8.52	34	96.4
Feb	6.07	29.3	67
Mar	10.6	13.85	22.4
Apr	26.96	31.56	102.4
May	15.72	27.32	42.5
Jun	67.38	100.17	58.9
Jul	30.49	43.29	51.6
Aug	100.58	78.55	130
Sep	90.86	58.36	237.7
Oct	129.27	358.44	308.1
Nov	43.75	102.9	176.2
Dec	16.25	105.1	82.5
Average	45.54	81.90	114.64
Std Dev	39.84	89.00	85.90

MM5 Variable Ranges	
K	E (m/yr)
0	0.36
0.5	0.39
1	0.42
1.5	0.46
2	0.49
2.5	0.52
3	0.55

Loss to ET (m^3/yr)	4.91E+07
Amount Left Over	4.93E+08
Annual % Water ET Loss	11.04

Residence Time Calculations

2017	Zone 1	Zone 2	Zone 3
Surface Area (m^2)	1.95E+06	7.88E+06	4.63E+07
Depth (m)	23.8	10	10
Volume (m^3)	4.64E+07	7.88E+07	4.63E+08
ET Loss (m^3/yr) Average	1.70E+06	6.86E+06	4.03E+07
Surface Inflow (m^3/yr)	0.00E+00	1.45E+08	2.03E+07
Surface Outflow (m^3/yr)	1.45E+08	2.30E+08	0.00E+00
Precipitation Inflow (m^3/yr)	8.42E+05	3.40E+06	2.00E+07
Bulk Inflow (m^3/yr) (w.o. cenote)	1.46E+08	1.48E+08	4.03E+07
Bulk Outflow (m^3/yr)	1.47E+08	2.37E+08	4.03E+07
Other Cenote Contribution	0	8.86E+07	0
Residence Time (yr)	0.32	0.33	11.49

2018	Zone 1	Zone 2	Zone 3
Surface Area (m^2)	1.95E+06	7.88E+06	4.63E+07
Depth (m)	23.8	10	10
Volume (m^3)	4.64E+07	7.88E+07	4.63E+08
ET Loss (m^3/yr) Average	1.81E+06	7.33E+06	4.31E+07
Surface Inflow (m^3/yr)	0.00E+00	1.77E+08	1.78E+07
Surface Outflow (m^3/yr)	1.77E+08	2.49E+08	0.00E+00
Precipitation Inflow (m^3/yr)	1.07E+06	4.31E+06	2.53E+07
Bulk Inflow (m^3/yr) (w.o. cenote)	1.78E+08	1.81E+08	4.31E+07
Bulk Outflow (m^3/yr)	1.78E+08	2.56E+08	4.31E+07
Other Cenote Contribution	0	7.56E+07	0
Residence Time (yr)	0.26	0.31	10.75

2019	Zone 1	Zone 2	Zone 3
Surface Area (m^2)	1.95E+06	7.88E+06	4.63E+07
Depth (m)	23.8	10	10
Volume (m^3)	4.64E+07	7.88E+07	4.63E+08
ET Loss (m^3/yr) Average	1.79E+06	7.25E+06	4.26E+07
Surface Inflow (m^3/yr)	0.00E+00	1.45E+08	-2.91E+06
Surface Outflow (m^3/yr)	1.45E+08	2.11E+08	0.00E+00
Precipitation Inflow (m^3/yr)	1.92E+06	7.74E+06	4.55E+07
Bulk Inflow (m^3/yr) (w.o. cenote)	1.47E+08	1.53E+08	4.26E+07
Bulk Outflow (m^3/yr)	1.47E+08	2.19E+08	4.26E+07
Other Cenote Contribution	0	6.57E+07	0

Residence Time (yr)	0.32	0.36	10.87

Average Inflow (m^3/yr)	4.71E+08	4.82E+08	1.26E+08
Average ET Loss (m^3/yr) Average	5.30E+06	2.14E+07	1.26E+08
Average Residence Time (yr)	0.30	0.33	11.04
Std Dev Tr	0.03	0.03	0.40

Overall E/I	0.14

Stream Gauge Data and Catchment Area Calculations

Year	Rapids (m^3/sec)	Chaac (m^3/sec)	Difference in Flow (%)	Rapids:Chaac Ratio (%)
2017	4.6	7.3	22.7	63.0
2018	5.6	7.9	17.0	70.9
2019	4.6	6.7	18.6	68.7

Year	Rapids Flow (m^3/yr)	Precipitation (m/yr)	Catchment Area (m^2)
2016		0.43171	
2017	145065600	0.54645	3.36E+08
2018	176601600	0.98284	3.23E+08
2019	145065600		1.48E+08

Carbon Isotope Sampling Data

2017-2018 Sampling	
Sampling Site	Delta 13 C
Las Palmas Small Spring	-9.99
Las Palmas Main Spring	-14.06
Las Palmas Main Spring	-12.00
Las Palmas Main Spring	-11.63
Xul Ha Spring	-11.18
Xul Ha Spring	-11.48
Mangrove Bay Sediment (Paradise)	-1.48
Mangrove Bay Sediment (Paradise)	-1.52
Mangrove Bay Oncoid	-0.85
Oncoid Sample (500m downstream of Gauging Station)	-1.03
Oncoid Sample (500m downstream of Gauging Station)	-1.11
Juan Carlos Well Cuttings	-0.39
Xul Ha Embayment	-7.49
Xul Ha Embayment	-7.41
Mid Lake	-9.55
Hotel Amigos Dock	-6.72
Hotel Amigos Dock	-6.78
Buena Vista	-6.78

2019 Sampling	
Sampling Site	Delta 13 C
CB19 10M	-8.66
CB19 10M	-8.57
CB19 30M	-9.40
CB19 30M	-9.64
CB19 50M	-9.85
CB19 50M	-9.78
BV19	-10.11
BV19	-10.48
LM19	-6.48
LM19	-6.70
ML19	-6.90
ML19	-7.24

Annual CO_2 Exsolvation and Calcite Precipitation Zone 1 Calculations

Calculation	CO2	Calcite
Amt Lost from Spring to Bay (mmol/L)	2.15	0.85
Inflow*Amt Loss (mol/yr)	1.01E+09	3.99E+08
Inflow*Amt Loss (kg/yr)	4.45E+07	3.99E+07

Calcite Annual Precipitation in Zone 1	
Calcite Density (kg/m^3)	2710
Precipitated Calcite (kg/yr)	3.99E+07
Zone 1 Surface Area (m^2)	1.95E+06
Volume Precipitated (m^3)	14737.23
Vertical Precipitation (m/yr)	0.0076
Uniform Precipitation Thickness (mm/yr)	7.558